UNIVERSITY OF OKLAHOMA

GRADUATE COLLEGE

EVALUATING DESERT SILT PRODUCTION USING FIELD, EXPERIMENTAL, AND REMOTE-SENSING METHODS

A THESIS

SUBMITTED TO THE GRADUATE FACULTY

in partial fulfillment of the requirements for the

Degree of

MASTER OF SCIENCE

By

STEVEN MICHAEL ADAMS
Norman, Oklahoma
2018

EVALUATING DESERT SILT PRODUCTION USING FIELD, EXPERIMENTAL, AND REMOTE-SENSING METHODS

A THESIS APPROVED FOR THE
CONOCOPHILLIPS SCHOOL OF GEOLOGY AND GEOPHYSICS

BY

_____
Dr. Gerilyn S. Soreghan, Chair

_____
Dr. Kirsten de Beurs

_____
Dr. Megan E. Elwood Madden

To my family, for their encouragement and support.

Acknowledgements

I would like to thank Dr. Lynn Soreghan for her mentorship and guidance. I am thankful to my committee members Dr. Kirsten de Beurs and Dr. Megan Elwood Madden for their review and recommendations. I would like to thank Joel Young for his assistance in constructing the experimental device used in this project. This work was funded in part by an SEM student grand and a GSA student grant.

Table of Contents

List of Tables

List of Figures

Abstract

Production of the silt that forms loess deposits has been attributed to processes operating in both glacial environments (via glacial grinding) and warm deserts (via saltation-induced fracturing). However, the efficacy of warm desert processes for major silt production remains controversial. Understanding the potential for silt production in desert environments is essential for determining the paleoclimatic significance of loess deposits. To better assess the significance of aeolian abrasion as a silt production mechanism, experimental abrasion was conducted in a device designed to enable saltation of sand (~100 g) at sustained storm wind velocities (~25 m/s). This design differs from previous studies in using 1) natural aeolian dune sand, 2) a relatively large starting mass, and 3) controlled wind velocities, and thus enables the scaling of results to natural geologic conditions. After experimental abrasion, produced silt had a mode (35.3 - 45.6 μm) which is in the range of typical North American Peoria loess, coarser than typically found in the Chinese Loess Plateau (25 μm) and finer than coarse modes found at desert margins in north Africa (>60 μm). Scaling rates of production from experimental results to the geologically significant scale indicates aeolian abrasion within deserts produces insufficient silt to create large loess deposits.

Introduction

Desert Loess Problem

The desert loess hypothesis proposes that silt particles in the range of 20-63μm originate by processes within deserts, and aeolian transport of these particles then form loess deposits (e.g., Smalley and Vita-Finzi, 1968; Smith et al., 2002). Based on the results of experimental work, processes for desert silt production are proposed to include both chemical and mechanical weathering (Wright, 2001a; Whalley et al., 1987). Aeolian abrasion of sand through saltation-induced grain collisions is hypothesized by some researchers to form substantial volumes of silt, and thus cited as a potential source for loess deposits (Tsoar and Pye, 1987; Crouvi et al., 2010). Results of saltation-induced silt production vary in laboratory simulations with different experimental designs producing negligible to substantial silt (Keunen and Perdock, 1962; Whalley et al., 1987; Smith et al., 1991; Wright, 2001; Bullard et al., 2007). In past glass-tube chamber experiments, the nature of the starting material varied, and the velocities of colliding grains were unknown (Bullard et al., 2004). Here, I test the desert loess hypothesis by (1) using a new abrasion device designed to replicate aeolian saltation, (2) using remote sensing and analytical techniques to study changes in sediment characteristics within a dune field, and (3) investigating potential differences between silt created by aeolian abrasion and silt transported into the dune field.

Significance of Desert Dust and Loess

Evaluating the potential of silt production in desert environments is fundamental to the use of loess deposits as a paleoclimate indicator. Silt that composes *most* of Earth's major loess deposits has been linked to glacial intervals and processes (e.g.,

Pye, 1995; Smalley, 1995; Assallay et al., 1998; Smalley et al., 2005, Muhs, 2013). The relative production of loess-sized particles from desert processes is unknown, although some assert it forms a significant amount (Wright, 2001b; Crouvi et al., 2010). Knowing the relative contribution of different processes to global silt production enables improved interpretations of depositional environments and climates of the past. If warm-desert processes produce large amounts of silt, then loess deposits in the geological record may have originated wholly or in part in warm deserts. If deserts do not produce a significant amount of silt in the loess range through aeolian abrasion, then desert-margin loess deposits likely contain silt produced by another mechanism. Such a result would strengthen the argument that large loess deposits are made of silt produced in glacial systems, and that silt production in deserts is relatively minor.

Dune sediments naturally contain a fraction of silt. Part of this fraction was likely transported into the dune field with the sand that forms the bulk of dune fields. If additional silt forms within a dune field through saltation-induced fracturing, then newly fractured silt may exhibit detectable characteristics distinct from allochthonous silt. Potential characteristic differences are investigated using spectral reflectance, grain size, and grain morphology analysis. This project tested a model (Figure 1) designed to distinguish between the relative amount of silt in a dune field that was allochthonous to the desert relative to the amount of silt produced through aeolian abrasion within the desert. The aim was to determine if the silt expelled by a desert is limited by an upwind sediment supply or if it is limited by silt production within the desert. The dust from deserts influences nutrient input to oceans and soils, and affects radiative forcing in the atmosphere (Goudie and Middleton, 2001; Crouvi et al., 2010). Assessing the relative

proportion of silt produced in desert field sites is also useful when interpreting experimental results.

Sediments naturally accumulate yellow to red-oxide coatings through a process known as rubification (Ben-Dor et al., 2006). In desert environments these coatings require on the order of 10^4 years to cover a quartz sand grain (Bullard and White, 2005). If a coated quartz grain is fractured and creates one or more silt particles, those particles will exhibit a fresh fracture face lacking a rubification coating. An allochthonous silt particle originally transported into the desert and undergoing rubification along with the sand grains would be similarly coated with oxides. This difference may allow the two types of silt grains to be distinguished optically. A population of completely coated silt grains compared with a population containing silt grains with fracture faces should exhibit different spectral reflectance patterns in the visible light range. Comparison with lab-produced end-member reflectance curves could thus reveal whether or not a silt population contains relatively high or low numbers of silt grains produced in the dune field by in situ saltation fracturing.

Allochthonous silt particles transported into deserts were likely produced by processes other than aeolian abrasion, such as glacial grinding, fluvial comminution, or chemical weathering. The processes that produced these silt grains might impart a signature on the grain morphology distinct from the morphology of silt grains produced through aeolian abrasion. To test this hypothesis I analyzed silt grains produced in an abrasion device for their similarity to silt produced in dune fields.

Differences in grain size and color might be detectable using remote sensing techniques on aerial and satellite imagery of desert dune fields (Ghrefat et al., 2007). If

a change in spectral redness is detected this would indicate an increase in fractured grains with clean faces or a removal of rubified grain coatings (White and Bullard, 2009). This project used high-resolution multispectral images and remote sensing techniques to produce surface reflectance curves along a downwind transect. Validation of reflectance curves was attempted with collected ground samples.

The goal of this study is to determine how much silt can be made under simulated natural conditions in a laboratory setting, and scale those results to geologically recognizable dimensions. Results of this scaling will reveal if desert environments are capable of producing significant and recognizable loess deposits assuming the experiment design is a reasonable representation of natural processes. Results are also analyzed for characteristics that may be diagnostic of their origin.

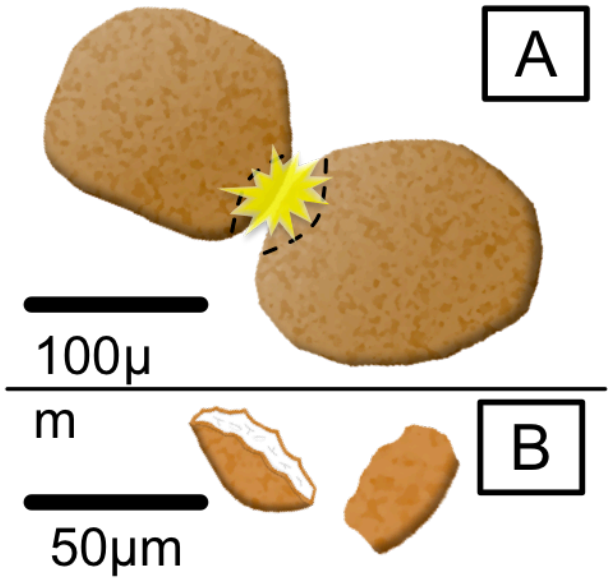

Figure 1: Silt Production From Grain Collision

(A) Schematic representation of a collision between two rubified (iron-oxide-coated) sand grains. (B) Silt grain (left) with fresh fracture face produced by intergranular collision. A completely coated silt grain (right) transported into the desert.

Background

Past Experiments

Previous studies used a variety of methods and starting materials to examine the effectiveness of aeolian abrasion in silt production. Kuenen (1960) used well-sorted quartz sand, crushed quartz, crushed feldspar, quartz cubes, and limestone cubes (0.4-4 mm) in aeolian abrasion chambers, and concluded that aeolian environments do not produce significant silt in the 10-50 μm range. In contrast, Whalley et al. (1987) used crushed Brazilian quartz of 350-500 μm in an air-agitated glass test tube, and found significant generation of silt. Smith et al. (1991) and Bullard et al. (2007) adapted the device used by Whalley et al. (1987), but with different starting materials—Pannonian sand (Smith et al., 1991), and dune sand from the Simpson Desert, Australia (Bullard et al., 2007), and both found initial production of silt that diminished with time, as the starting material rounded, and diminished in size. A caveat to the Bullard et al. (2007) results is that the authors did not sieve the starting material to remove any pre-existing silt, and they used samples that included pre-existing clay coatings.

Table 1. Past Experimental Results

Author	Year	Abraded Material	Device	Time Abraded (hours)	Starting Mass (g)	% Of Starting Mass[†]
Kuenen	1960	Limestone and Quartz	3 Devices	N/A	N/A	0
Whalley et al.	1987	Crushed vein quartz (350-500 μm)	Test tube	48	12g	54
Smith et al.	1991	Miocene marine sand (350-500 μm)	Test tube	128	10g	1.86
Wright	1993[††]	Fluvial Sands	Test tube	204	10g	0.063
Wright et al.	1998	Crushed vein quartz (250-500 μm)	Test tube	96	10g	28.7
Bullard et al.	2004	Dune sand unfiltered	Test tube	120	10g	2.3
		Dune sand >250 μm	Test tube	120	10g	0.263

Note: Keunen used three abrasion devices (circuit tunnel, circuit tube, and wind tunnel) and different material for abrasion in his experiments (polished river sand, crushed quartz, crushed feldspar, quartz cubes, and limestone cubes)

[†]Silt mass produced as a percent of the original starting mass

[††]From Wright, 2001a. Cited from an unpublished thesis from 1993 in 2001 by (Wright, 2001a)

Table 1. Results of past aeolian abrasion experiments ordered by year conducted.

Previous Remote Sensing Studies

Many authors have studied sediment grain size using remote sensing platforms (Leu, 1977; Okin, and Painter, 2004; Ghrefat et al., 2007; Lv and Sun, 2016). Spectral reflectance curves vary with changes in grain size and mineralogy. However, the influences of topography, and of sediment of varying grain size and composition make it difficult to estimate grain size with remote sensing alone (Leu, 1977; Okin and Painter, 2004). A shift in reflectance curves was observed with a change in distance along a sand plume, indicating that grain-size shifts can be distinguished with hyperspectral images (Okin and Painter, 2004). Maps of granulometry were successfully produced in the gypsum dunes at White Sands owing to the uniform mineralogy (Ghrefat et al., 2007). White and Bullard (2009) observed that sediment in stable dunes exhibited a decrease in redness with distance transported down wind. The decrease in redness by clay coating loss was replicated by abrading sand in the same glass test tube chamber used by Bullard et al. (2007) and Whalley et al. (1987). This current project seeks to determine if changes in dune sediment redness are from fracturing of grains, from chipping of clay coatings, or both.

Geological Background and Sample Sites

Sediment samples were collected for study from active aeolian dunes in the Little Sahara State Park in Oklahoma (Figure. 2). The dunes are composed of orange to red-oxide- and clay-coated sand, suitable for testing the silt-fracture hypothesis experimentally. The stable dunes of the Cimarron River Valley are hypothesized to

redden with age, although eroded red Permian age silt and clay may also affect the color where they mix by coating the sand (Lepper and Scott, 2005).

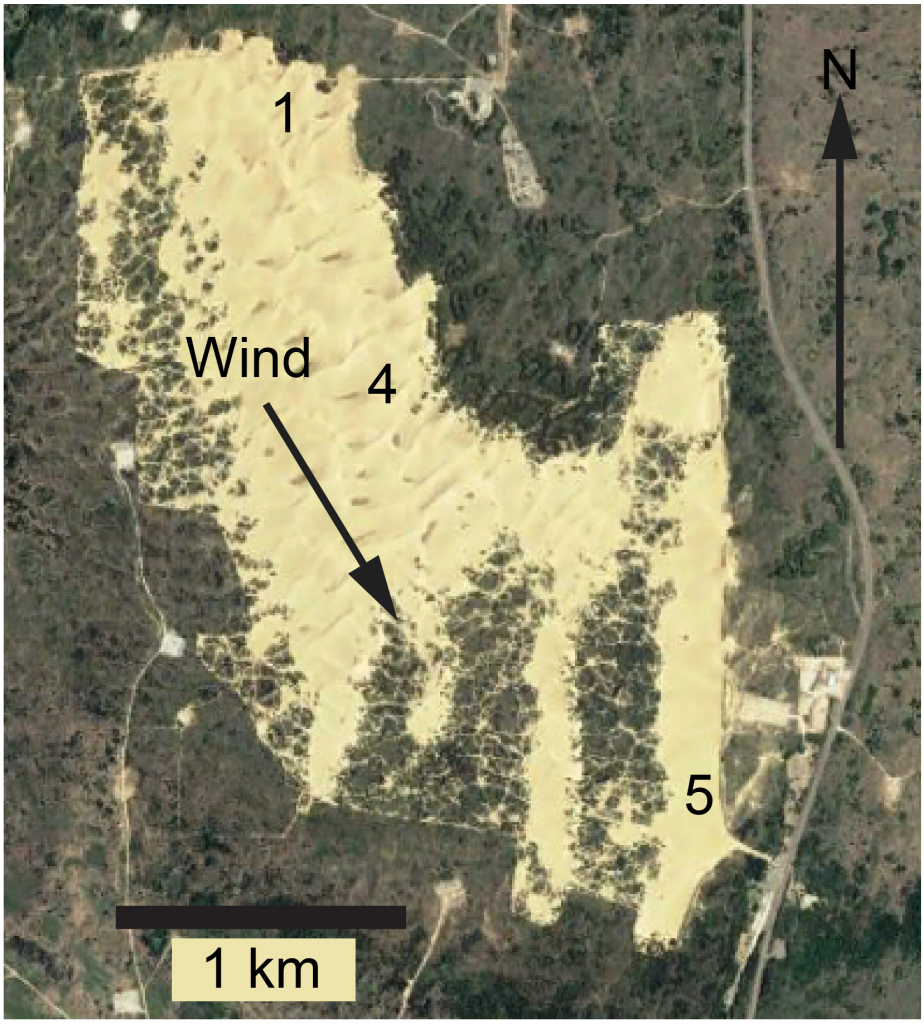

Figure 2. Little Sahara, Oklahoma Field Area

Sample collection sites along a down wind transect. Five samples were collected. The three displayed are the samples used for grain-size analysis. The upwind (1), mid-dune field (4), and downwind (5), sample sites were selected to highlight downwind changes in grain size. The upwind site (1) had a large sample collected and was used as starting material in the abrasion device. Sample sites correspond to samples LS-S1, LS-S4, and LS-S5.

The semi-active dunes of the Little Sahara State Park form part of the Cimarron River valley dune system. The dune field developed in the Holocene and was active as recently as the 1930s Dust Bowl (Rogers, 2000). More recently, vegetation has stabilized many of the dunes, but those in Little Sahara State Park remain unvegetated owing to continual anthropogenic disturbance (motorized vehicle usage). The modern winds are bimodal, blowing from the NW and SW. The large linear dune crests are aligned with the adjacent stable dunes and appear to record predominant northwesterly paleowinds (Rogers, 2000).

Additionally, dune sand is studied from the Algodones Dune field located in the Imperial Sand Dunes Recreational Area of southern California (Figure. 3). The dune field stretches 80 km along a NW to SE path, and ranges from 3 km wide in the NW to 10 km wide in the SE, reflecting northwesterly prevailing winds (Muhs et al., 1995; Derickson et al., 2008). The sediment of the Algodones dune field was supplied by the Colorado River from the late Pleistocene through the Holocene when the Colorado River periodically diverted into the Salton Trough, delivering sediment to the shores of paleolake Cahuilla (Stokes et al., 1997). The latest natural diversion of the Colorado River was approximately 400 years ago (Muhs et al., 1995). Derickson et al. (2008) designated four zones in the dune field, characterized by different dune morphologies, and hypothesized that the dunes were emplaced sequentially from east to west along the distal alluvial fans of the Chocolate Mountain, supplied by the shore of paleolake Cahuilla, which was just west of the dune field. The sediments are light yellow to brown in color and test the limits of the model for detecting subtle changes in grain reflectance spectra. Pye and Tsoar (2013) noted that differences in mean grain size

between the lee sides of dunes and the stoss side-interdune can be detected from the air by subtle color changes.

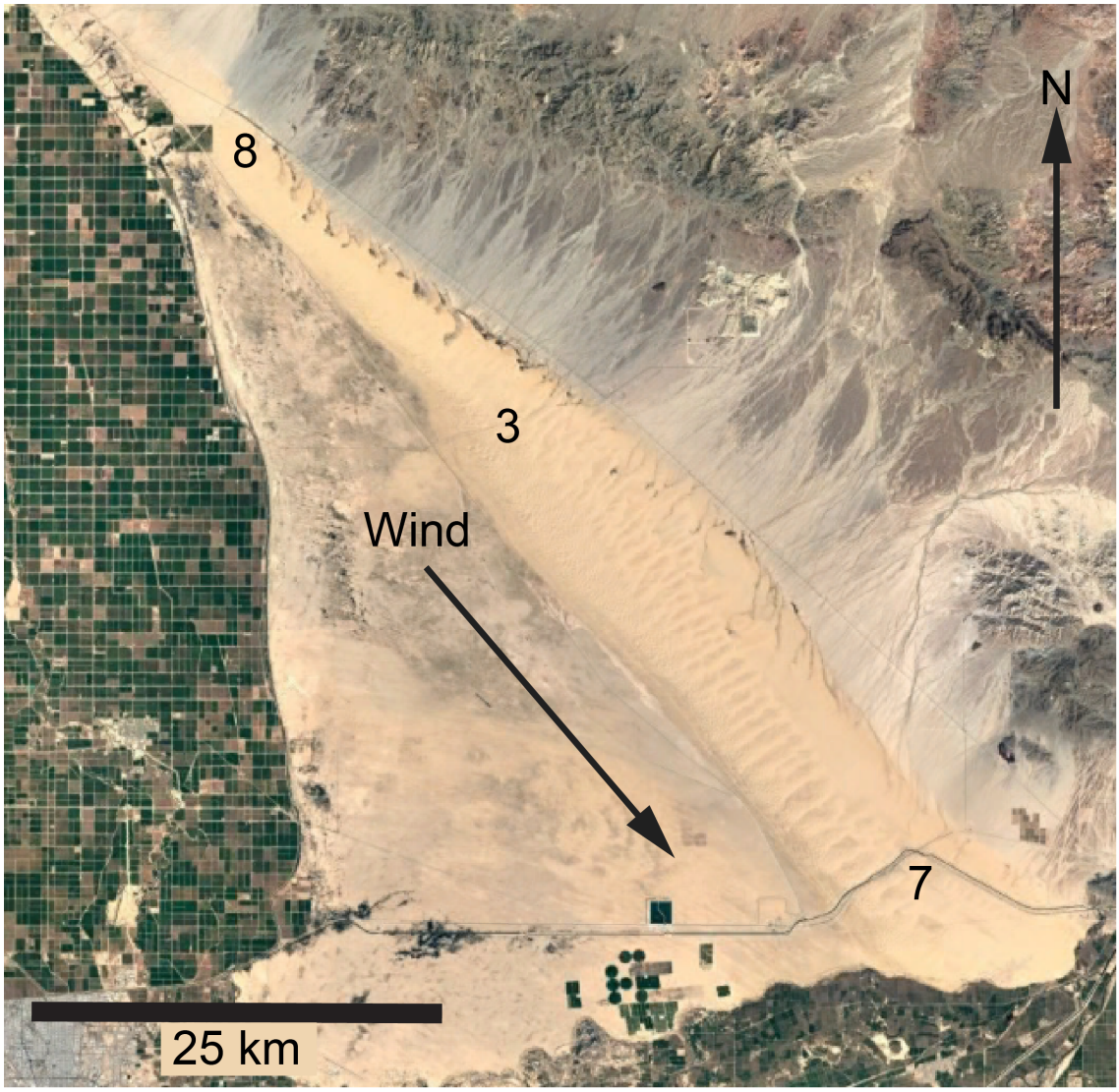

Figure 3. Algodones, California Dune Field Area

Sample collection sites along a down wind transect of the Algodones dune field, California. Eight samples were collected. The upwind (8), mid-dune field (3), and downwind (7) sample sites were selected to highlight downwind changes in grain size. The upwind site (8) had a large sample collected and was used as starting material in the abrasion device. Sample sites correspond with samples AL-S8, AL-S3, and AL-S7.

Methods

Sample Collection

Dune sediments were collected for aeolian abrasion experiments and analysis of physical and spectroscopic changes arising from downwind transport. Samples of ~2 kg were collected from the dune crests of upwind dune sites (sample site 1 in Figure 2, sample site 8 in Figure 3) and used for starting material in aeolian abrasion experiments. To investigate sediments altered by different lengths of transport, samples were collected along downwind transects at both field sites. One 2 kg upwind sample and five ~200 g transect samples were collected from the Little Sahara State Park dune field (Figure 2). All samples from the Little Sahara State Park dune field were collected from dune crests. Similarly, one upwind sample and eight transect samples were collected from the Algodones dune field (Figure 3). Samples 1, 2, 3, 4, 7, and 8 were collected from dune crests. Samples 5 and 6 were collected from coarse deflated surfaces.

Sample Preparation

Transect samples were divided in half with a riffled sample splitter. One half of each site sample was used for spectroscopic analysis. The other half was used for grain-size analysis. The sample for grain-size analysis was sieved to >250 μm, 63-250 μm, and <63 μm fractions, taking care to collect all fractions. The <63 μm fraction was measured with the Mastersizer 3000 laser particle-size analyzer (LPSA).

The 2 kg upwind site samples were sieved to remove grains <250 μm. Once sieved the >250 μm fraction was split. One half was designated as original starting material (”unwashed fraction”), the other (designated “washed fraction”) was washed in a 5% sodium hexametaphosphate dispersant for 10 minutes to remove surface grain coatings.

After washing with dispersant the sand was rinsed three times with distilled water and dried in an oven at 90° C. The >250 μm fraction of the original fraction and the washed fraction was then divided into 100 g aliquots for use as starting samples in the abrasion device. For each of the starting material types (Algodones washed, Algodones original, Little Sahara washed, and Little Sahara original), four 100 g samples were produced for abrasion in the experimental device and one 100 g sample was used as a control. The control sample was post processed by the same methods as the samples used in the experimental device. The four 100 g samples were designated for one-, two-, four-, and eight-day abrasion tests.

Abrasion Device

The experimental abrasion device (Figure 4) creates airflow with a range of 3-35 m/s in a sub vertical (60^{o} inclination) 5-cm diameter polycarbonate tube chamber. The chamber has a 120 μm steel mesh filter at the base and a 5 μm steel mesh filter at the top. The top filter is cylindrical with two 5 μm steel mesh covered openings (10 × 3 cm). The filter penetrates 30 cm into the top of the chamber. This design prevents clogging of the upper filter by accumulating sand, which occurred during initial tests using a flat upper filter. Whereas grains <5 μm technically can pass through the upper filter, they typically do not; rather, clay-size particles accumulate on the chamber side of the filter owing to electrostatic formation of aggregates >5 μm. Sand samples placed in the chamber prior to operation settle into a pseudo-dune, wedge shape partially blocking airflow through the chamber (Figure 5). The device is powered by two vacuum motors, each with voltage regulators.

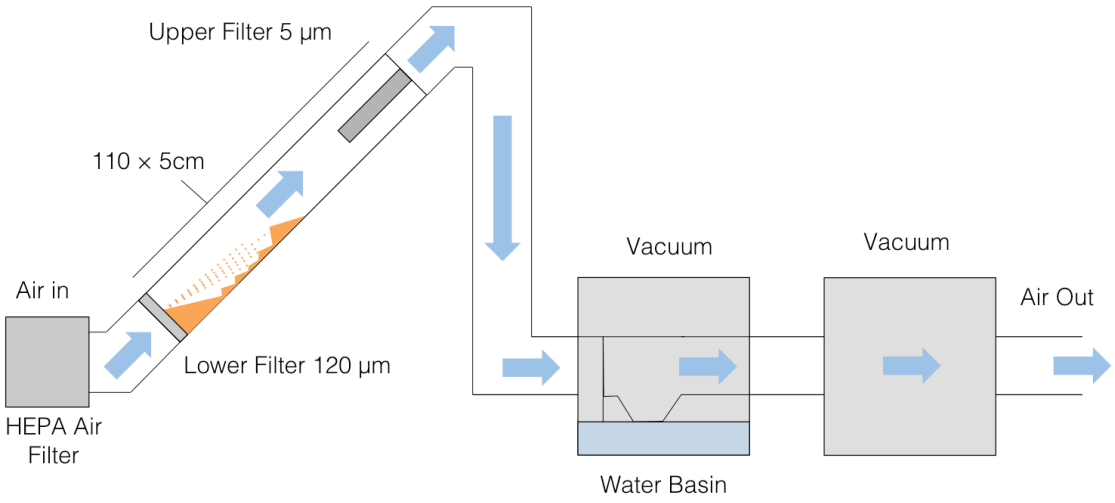

Figure 4. Schematic Diagram of Experimental Abrasion Device

Figure is not to scale. Chamber width is 5 cm. Chamber length is 1.1 m. Lower filter is a flat 120 µm steel mesh. Upper filter is 5 µm steel mesh around a 3 cm diameter PVC cylinder. Two vacuum motors generate airflow. Air pulled into the system is filtered by a HEPA filter to prevent contamination. Abrading sediment rests on the 120 µm steel mesh filter at the bottom of the abrasion chamber. Abrading sand forms a small wedge from which sand is blown upwards in the chamber. As sand rolls back down the chamber toward the wedge additional sand is blown from below into those sand grains creating collisions. Fine grains produced through abrasion in the chamber are trapped by the 5 µm upper steel mesh filter. Particles smaller than 5 µm did not pass through the upper filter as they typically form small particle aggregates > 5 µm. An average wind speed of 25 m/s was maintained by adjusting the power of both vacuums periodically. Adjustments to vacuum motor power had to be made roughly twice a day due to the slow accumulation of fines on the upper 5 µm filter, which slowed air flow and wind speed.

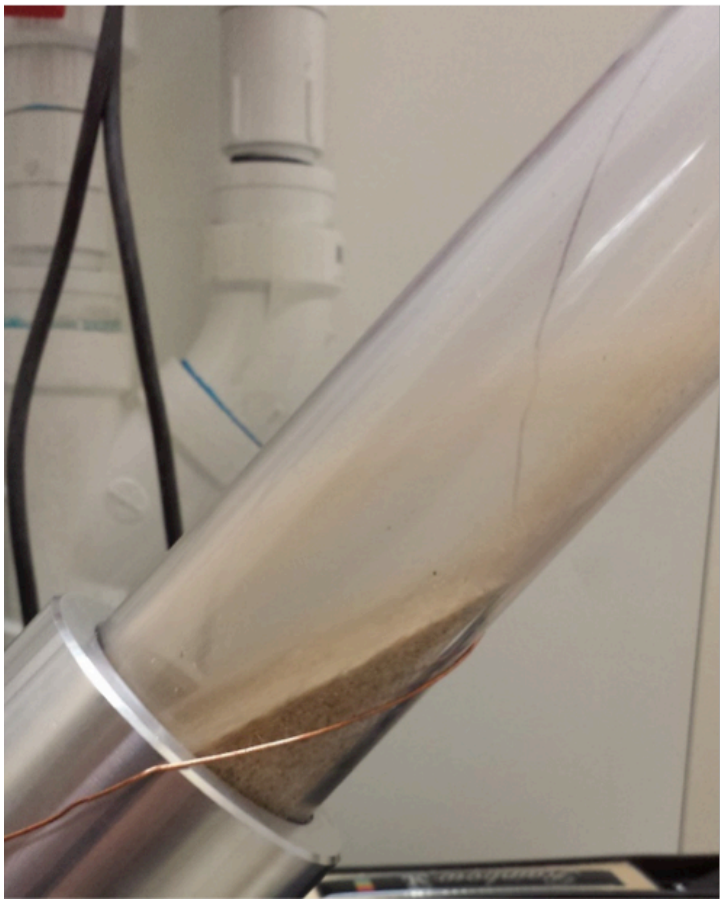

Figure 5. Photo of Abrading Sand at Base of Chamber

Chamber width is 5 cm. Sand forms a small wedge at the base of the chamber. Sand is blown from the base of the wedge where the sand constricts the flow the greatest and velocity is highest. Small piles of sand fall back toward the sand wedge and collide with sand being blown upward from below.

Air velocity was measured using a hotwire anemometer with and without sand present in the chamber to determine the range of velocities possible and the throw of the sand grains under those conditions. The device is capable of creating higher wind velocities, however in the highest-velocity setting(s) all of the sand accumulates at the top of the chamber. To maintain a cycle of sand continually saltating at the base of the chamber, experimental velocities did not exceed 25 m/s. Wind velocities vary slightly during testing owing to shifting of the sand wedge that constricts the airflow of the chamber to varying degrees. When the chamber diameter becomes restricted, the velocity increases and more sand blows upward, reducing the restriction and decreasing the chamber velocity. This periodic cycling of constriction and free flow repeats roughly twice per second.

Due to the variable nature of the sediment wedge and the slow accumulation of clay on the top filter both vacuum motors were monitored and adjusted periodically to maintain an abrasion cycle with wind velocities in the range of 25 m/s. This was accomplished by placing markers on the chamber for the maximum and minimum throw range of sand under ~25 m/s conditions and adjusting the vacuum motors to fit this range. A peak wind speed of 25 m/s was selected because it is the velocity experienced during severe dust storms (Zijiang and Xiwen, 2002).

Testing Intervals and Data Collection

Abrasion tests for the original and washed fractions from the Little Sahara and Algodones field sites were conducted for one-, two-, four-, and eight days. Sample sizes of 100 g consisting of particles >250 μm were placed at the bottom of the abrasion

chamber on the 120 μm mesh and the chamber was sealed. Both vacuum motors were powered on to induce grain movement and adjusted to bring the abrasion cycle within the 25 m/s range.

Abrasion resulted in removal of clay coatings, and this clay then accumulated on the upper 5 μm filter. If the abrasion test continued beyond two days the upper filter was removed and cleaned every two days. The clay was collected by rinsing the filter with distilled water and using a nylon brush to dislodge the clay. After the filter was cleaned and dried it was replaced and the abrasion test was resumed. Dust removed from the filter was later processed along with the coarser sand from the chamber for grain-size analysis.

At the end of the experiment the upper filter was removed and the dust collected. The dry sediment in the chamber was poured out, the bottom mesh filter removed, and the chamber tube rinsed with distilled water into a beaker. After sediment was collected from the chamber and rinsed from the filters, the chamber and filters were washed using Dawn soap and water. Washed components were rinsed in distilled water and dried with compressed air and microfiber cloths.

The abrasion of sand particles in the polycarbonate chamber generated static electricity, causing clinging of grains to chamber walls, and slow grain migration upwards. To prevent this, a commercial anti-static spray (Static Guard) was sprayed into the chamber after cleaning.

Post Processing of Abraded Samples

Silt Removal

Samples from the abrasion device consisted of fine particles rinsed from the chamber and filter, and the dry component from the chamber. The wet collected fraction was left to settle for 24 hours in a large covered beaker. After 24 hours excess water was siphoned out of the beaker with a pipette. The dry sediment was dry sieved for 15 minutes in a manual crank sieve shaker. The sieves used were 250 μm and 63 μm. After dry sieving the sediment was wet sieved using the same sieves. Water and particles passing through the 63 μm sieve were collected in a large beaker and left to settle for 24 hours. The >250 μm and 63-250 μm fractions were collected and dried at 90 ^{o}C in an oven, then cooled and weighed.

The <63 μm fraction was collected from the beaker and placed into 50 mL centrifuge tubes and centrifuged at 4500 rpm for 40 minutes. Excess water was removed from the centrifuge tubes, and the sediment consolidated to one tube and centrifuged again at 4500 rpm for 40 minutes. Separation of the clay and silt fractions was aided by adding 3% sodium hexametaphosphate to the centrifuge tube, mixing, and pipetting the resultant slurry through a 5 μm steel mesh sieve.

The silt remaining on the sieve was rinsed with distilled water over a vacuum flask to remove remaining clay (also silt between 4 and 5 μm). The silt grains remaining on the 5 μm sieve were removed by rinsing with distilled water and placed in a 50 mL centrifuge tube and centrifuging for 10 minutes. Excess water was removed, and the silt was dried in a 90^{o} oven, cooled, and weighed (Figure 6).

Silt Size Analysis

Silt grains from the abrasion tests and control samples were analyzed using the Small-Volume (SV) Module on a Malvern Mastersizer 3000 laser particle-size analyzer (LPSA). Samples were placed in 20 ml glass vials and 1 ml of distilled water was added to the sample. The SV Module has a 7 ml glass chamber in which the samples were measured. 6 ml of distilled water was added to the measuring chamber and the chamber was loaded into the Mastersizer 3000. A background measurement was made to ensure the chamber was clean and that the background interference was low.

A pipet was used to agitate the sample and 1 ml of water in the glass vial to create a slurry in the pipet. The sample slurry was added to the chamber for measurement with a 1 ml pipet. The chamber was agitated with a magnetic stirrer, which spun at 700 rpm. After the sample was added three measurements were made and averaged. The volume percent and number percent for grains ranging in size from 0.01 to 1000 μm were calculated. These data are shown in Table 4 and Figures 7.

Spectroscopic Analysis

Sample spectral profiles were measured to investigate transport changes due to grain coating loss and grain chipping. Samples from the downwind transects were measured for comparison with experimental results. Experimental control samples were measured to represent the profile of the starting material. The >250 μm sand fraction of each sample post-abrasion was measured to study changes with abrasion time.

Hyperspectral profiles of samples were measured using a Lumini One Spectrometer. The Lumini One has a resolution of 8 nm and covers bands from 330 to 890 nm (Lumini ONE, 2018). Percent reflectance was calculated using a reflectance

standard. 250 ms exposures under identical lighting conditions were used for all samples. Samples were placed in a flat glass petri dish so that the surface of the sand was flat. Samples were measured 1 cm from the spectrometer aperture. Five measurements from each sample were taken and averaged.

Remote Sensing Method

A L1-C Sentinel-2 tile (10 m resolution) covering the Algodones Dune field from 2 March 2018 was acquired from USGS Earth Explorer. The L1-C product provides Top of Atmosphere (TOA) reflectance at 10 m resolution. This L1-C product was processed to Level 2A Bottom of Atmosphere (BOA) using the Sen2Cor toolbox in SNAP (SNAP, 2018). The Level 2A product provides atmospheric and terrain correction. The level 2A product is BOA reflectance with a quantification value of 10000.

Using the ENVI bandmath tool false color images were produced to look for changes in grain coatings throughout the Algodones Dune Field. False color images were created using spectral indices that have been shown to represent sediment grain coatings. The three spectral indices and their bandmath formulas are below for Red: 665 nm, Green: 560 nm, Blue: 490 nm, NIR: 842 nm SWIR: 1610 nm (ESA, 2015)

The Redness Index investigated by Mathieu et al., (1998) has been used in several studies to examine changes in sand grain coatings and this index has been used successfully in desert environments to show color variation across regions (Ben-Dor et al., 2006; White and Bullard, 2009; Roskin et al., 2012). The Iron Oxide ratio shows changes in iron oxide (hematite and goethite) content of an area (van der Meer et al., 2012). Iron oxides are assumed to be a component of the grain coatings in the study

area. The Ferrous Minerals Ratio shows areas with abundant ferrous minerals (van der Meer et al., 2012)

(1) *Redness Index:* $R^2 / B \times G^3$ (Mathieu et al., 1998)

(2) *Iron Oxide ratio:* R / B (van der Meer et al., 2012)

(3) *Ferrous Minerals Ratio:* $SWIR / NIR$ (van der Meer et al., 2012)

Color gradient images were created by restricting the upper and lower index values to those present in the dune field (Figures 9, 11, and 13). This restriction produced the greatest degree of variation for index values in the dune field. Four polygons were made to represent upwind, mid dune field, and downwind regions (Figure 9). Polygons were drawn to avoid vegetation and were drawn to cover only the large central dunes. The range of the color gradient was split into 16 bins and histograms were plotted to show the percent of pixels present in each bin. The ranges and bin sizes for the color slices in each image are in Table 2. Histograms showing percent of pixels were created for each of the four polygons (Figures 10, 12, and 14). This method was applied for the three images that resulted from the calculated indices.

Table 2. Bin Size and Range

Index	Bin Size	Value Range
Ferrous Minerals Index	0.0125	1.2-1.4
Iron Oxide Ratio	0.05625	1.5-2.4
Redness Index	3.75	20-80

Scaling Method

Assessing the potential for silt production from aeolian abrasion under conditions comparable to those at the geologic scale requires scaling up the experimental conditions to the dimensions of a large dune field. To achieve this, calculations were made to scale up both temporal and spatial aspects. A range of time intervals for the natural equivalent to eight days in the abrasion chamber were used based on studies of windstorm frequency and wind speed in regions with frequent severe dust stroms. The Ordos Plateau (Liu et al., 2005), between the Badain Jaran Desert and the Tengger Desert (Yang et al., 2014), and the Xinjiang region (Yao et al., 2012) are regions that have frequent dust storms and may supply the Chinese Loess Plateau with dust.

The assumptions used to scale up experimental results are based on available literature from natural systems. The rate of silt production in a natural system depends on the mass of sand active in abrasion, and the length of abrasion time. Scaling results up to those of a regional desert requires an estimate for the abrading sand mass (100 g in the experiment). For this calculation the variables required are: Desert Area (A), depth of abrading sand volume (h), and density of dune sand (D). The Namib Erg was chosen as a model location because it consists of a large continuous dune field for which a total area is easily measured using Google Earth (32,385 km^2). We assume that the depth of the actively saltating layer during a storm is less than or equal to the height of typical wind ripples which are approximately 10 to 20 times grain diameters and should typically not exceed 0.5 cm (Werner and Gillespie, 1993). A range of values for this depth variable were used to determine if exaggerated values had a significant effect.

A calculation of saltation mass was made to verify that the estimated abrading mass based on ripple height was reasonable.

Saltation mass is calculated from the maximum shear velocity (u*) expected during experimental abrasion. We assume this maximum shear velocity approximates the shear velocity experienced during wind storm gales; accordingly, equation (4) is solved for u*. A maximum wind speed of 30 m/s at a height of 2 cm above the surface yields a shear velocity of 1.5 m/s. A shear velocity of 1.5 m/s implies a saltating particle load of <400 g/m^2 (Kok and Renno, 2008). Multiplying this saltating particle load over the desert area gives the saltating mass during a gale with a wind speed 2 cm above the bed, in this case ~4×10^{12}g. The active abrasion mass calculated for a depth of 0.25 cm is 1.33×10^{14}g. As the active abrasion mass for 0.25 cm exceeds the saltating mass it is reasonable to assume that 0.25 cm is the maximum active abrasion depth.

(4) $U = (u^*/k) \ln(z/z_0)$ (Li et al., 2010)

u* - shear velocity

U - wind velocity = 30 m/s (max)

k - von Karman's constant = 0.4 (Kok et al., 2012)

z - height above surface = 0.02 m

z0 - surface roughness = D/30 (Kok et al., 2012)

D - grain diameter = 0.00025 m

Sand and silt densities are used to calculate the masses for the actively abrading volume and the theoretical silt deposit described below. Sand density was measured in the lab and determined to be 1.64 g/cm^3 for the Algodones site.

Mass of Namib Erg (MNE)

(5) MNE = area desert (A) x active depth (h) x density of sand (D)

To determine the extent of a geologically significant deposit, we use the area of the Chinese Loess Plateau relative to the area of adjacent deserts (~30% of the desert using the map of Pullen et al., 2011) and take one meter as a minimum mapable thickness (based on maps of LGM loess of North America from Bettis et al., 2003). Hence, a theoretical deposit of 1 m thickness and 10,000 km^2 is considered geologically significant.

The silt density measured in the lab was lower than typically used for Mass Accumulation Rates (MARs), so 1.65 g/cm^3 was used (Frechen et al., 2003)

Mass of Target Silt Deposit (TSD)

(6) TSD = area of deposit (A) x depth of deposit (h) x density of silt (D)

TSD = 1×10^{14} cm^2 x 100 cm x 1.65 g/cm^3

TSD = 1.65×10^{16} g

Target % = TSD / MNE

The rate of silt production is based on the amount of silt made relative to the starting mass of the abrading sample (100 g), therefore a percent of the abrading mass is used as the target mass of the silt deposit. Because deserts are able to constantly resupply the abrading mass the target percent can exceed the mass of the abrading desert fraction. If the depth of abrading sand is shallow (0.25 cm) and the starting mass is small the eventual silt deposit mass with a 1 m thickness will exceed the magnitude of the abrading sand mass.

The length of natural abrasion time represented by the 8-day experiments is challenging to estimate. The study by Liu et al. (2005) from the Ordos Plateau indicates that eight days in the chamber is equal to ~192 years at that location. Work by Yang et al. (2014) measuring wind data in between the Badain Jaran Desert and the Tengger Desert show that, measured annually, time spent at wind speeds near those in the abrasion (17 m/s) chamber is roughly 80 hours annually. This region is a corridor between deserts and may not be representative of the wind regime of the dune fields. The Xinjiang region has more potential for annual abrasion. The region is frequented by storms bringing gale-force winds over 17 m/s, and gusts up to 60 m/s, however the total time at those speeds is unknown (Cheng et al., 2015). Extreme wind event days with winds of 17 m/s or greater occur 100 days a year in some parts of the Xinjiang region (Yao et al., 2012). Based on these studies a maximum 8 day equivalence of 1 year is considered reasonable.

Table 3. Scaling Model

Experimental scale	Desert scale
Abrading sand mass = 100 g	Abrading sand mass = Varies with abrading depth (0.25 - 5 cm)[†]
Abrasion time at 20 m/s = 8 days (192 hours)	Abrasion time at 20 m/s = Annual hours (1 to 192)[††]
Maximum silt produced = 0.0037 g (0.0037% of starting mass)	Constant silt mass of 1.64×10^{16} g = Percent of starting mass[†††]

[†] Range of values for the abrading sand depth. Justification for this range in Methods

[††] When annual abrasion time at 20 m/s in the desert is 1 hour then 8 days in the experimental device = 192 years. When annual abrasion time at 20 m/s in the desert is 192 hours then 8 days in the experimental device = 1 year in the desert. The range of 1 to 192 annual hours was selected based on measured time intervals at this velocity by (Liu et al., 2005) for the lower limit and a the upper limit was selected to investigate how silt production changed with a much longer interval of abrasion.

[†††] Varies based on the abrading depth and magnitude of the starting mass

Table 3. Scaling model. Experiment scale variables are in the left column. Desert scale variables are in the right column.

Results

Table 4. Silt Mass and Grain Size Mode

Sample	Number of Days	Silt Mass (g)[†]	Grain size (µm)	
			Volume % Mode	Number % Mode
Algodones Washed				
AL-WS-C	0	0.0000	BDL	BDL
AL-WS-1D	1	0.0000	BDL	BDL
AL-WS-2D	2	0.0019	58.9	2.27
AL-WS-4D2	4	0.0014	45.6	2.00
AL-WS-8D	8	0.0037	35.3	2.00
Algodones Unwashed				
AL-OR-C	0	0.0000	BDL	BDL
AL-OR-1D	1	0.0002	BDL	BDL
AL-OR-2D	2	0.0003	BDL	BDL
AL-OR-4D2	4	0.0010	31.1	2.27
AL-OR-8D	8	0.0011	40.1	2.00
Little Sahara Washed				
LS-WS-C	0	0.0000	BDL	BDL
LS-WS-1D	1	0.0001	BDL	BDL
LS-WS-2D	2	0.0001	BDL	BDL
LS-WS-4D2	4	0.0026	51.8	1.759
LS-WS-8D	8	0.0036	45.6	1.999
Little Sahara Unwashed				
LS-RD-C	0	0.0004	BDL	BDL
LS-RD-1D	1	0.0000	BDL	BDL
LS-RD-2D	2	0.0009	35.3	2.00
LS-RD-4D	4	0.0011	27.4	2.27
LS-RD-8D	8	0.0025	35.3	2.00
Algodones Field Sites				
AL-S8	NA	NA	76.0	62.8
AL-S3	NA	NA	76.0	55.2
AL-S7	NA	NA	66.9	2.27
Little Sahara Field Sites				
LS-S1	NA	NA	66.9	55.2
LS-S4	NA	NA	76.0	62.8
LS-S5	NA	NA	76.0	62.8

BDL = below detectable level
NA = not applicable
WS indicates Washed samples
RD and OR indicate Unwashed samples
[†]Note: The starting mass was 100g, making the Silt Mas Produced in grams equivalent to the % of starting mass. % of starting mass is used as a metric of silt produced in previous studies

Table 4. Abrasion samples ordered by length of abrasion experiment, showing silt mass produced along with grain size displayed as number and volume percent modes. Field collected sites ordered from upwind to down wind showing silt grain size displayed as volume and number percent modes.

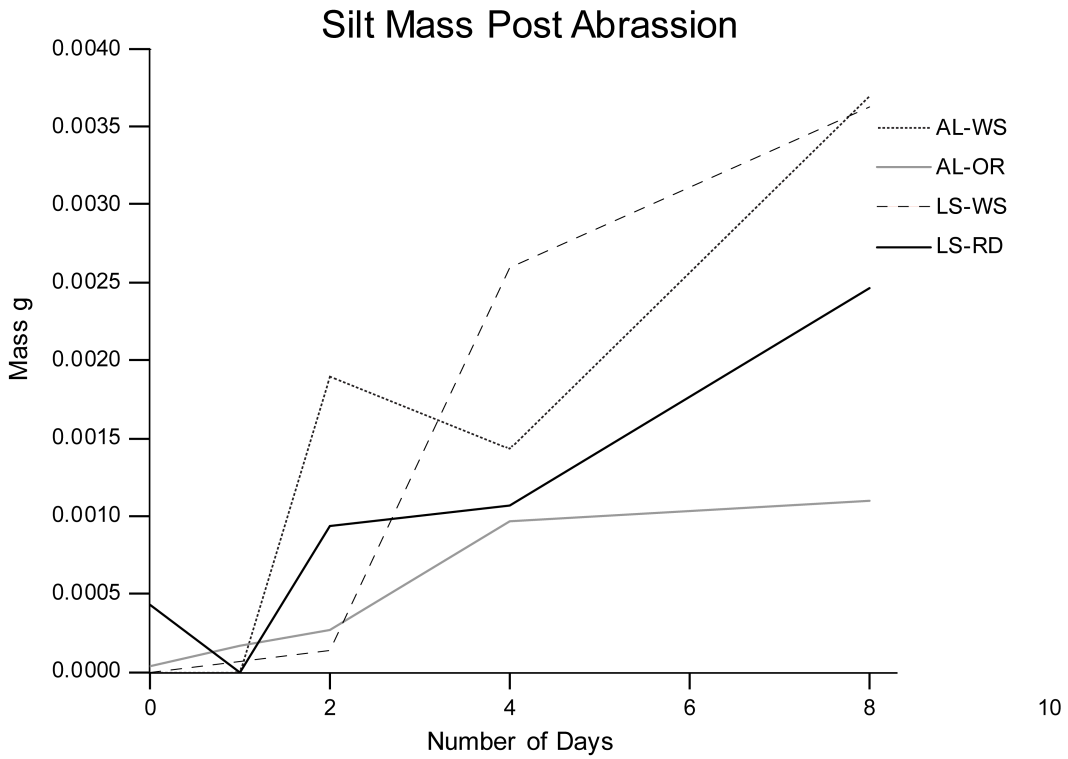

Figure 6. Silt Mass Post Abrasion

Mass produced after 1-day, 2-day, 4-day, and 8-day abrasion experiments. Controls are plotted at 0 on the x-axis. Algodones Washed (AL-WS), Algodones Unwashed (AL-OR), Little Sahara Washed (LS-WS), Little Sahara Unwashed (LS-RD).

Mass Results

Abrasion tests produced silt (~5-63 μm) with masses ranging from below detectable levels (BDL; defined here as <0.0001 g) to 0.0037g (Table 4 and Figure 6). Because the starting mass of abrasion tests was 100g, the silt mass produced in grams is equivalent to the percent of the starting material. Three control samples returned BDL masses and the unwashed Little Sahara control contained 0.0004 g of silt (0.0004% of starting mass). Abrasion tests lasting one day produced two BDL samples and two measurable samples. One-day tests showed little variation in the mass produced. Mass results for both of the 1-day abrasion intervals were less than the silt contained in the unwashed Little Sahara control. All 2-day tests produced measureable silt with masses of 0.0001 to 0.0019 g; two sample masses fell below the unwashed Little Sahara control. Four-day tests produced silt in all samples, with masses from 0.0010 to 0.0026 g. Of these, three produced less silt than the largest 2-day tests. The washed Algodones 2-day sample produced more silt than three of the 4-day abrasion interval samples. The washed Algodones 4-day sample produced more silt than the unwashed Algodones and Little Sahara 8-day samples. Eight-day abrasion intervals produced silt masses from 0.011 to 0.0037 g. For each individual sample type and location, the 8-day abrasion intervals produced more silt than the 4-day intervals. Washed samples produced more silt than unwashed samples for 4-day and 8-day abrasion intervals. Mass of silt produced increases with length of abrasion.

Silt Grain Size Results

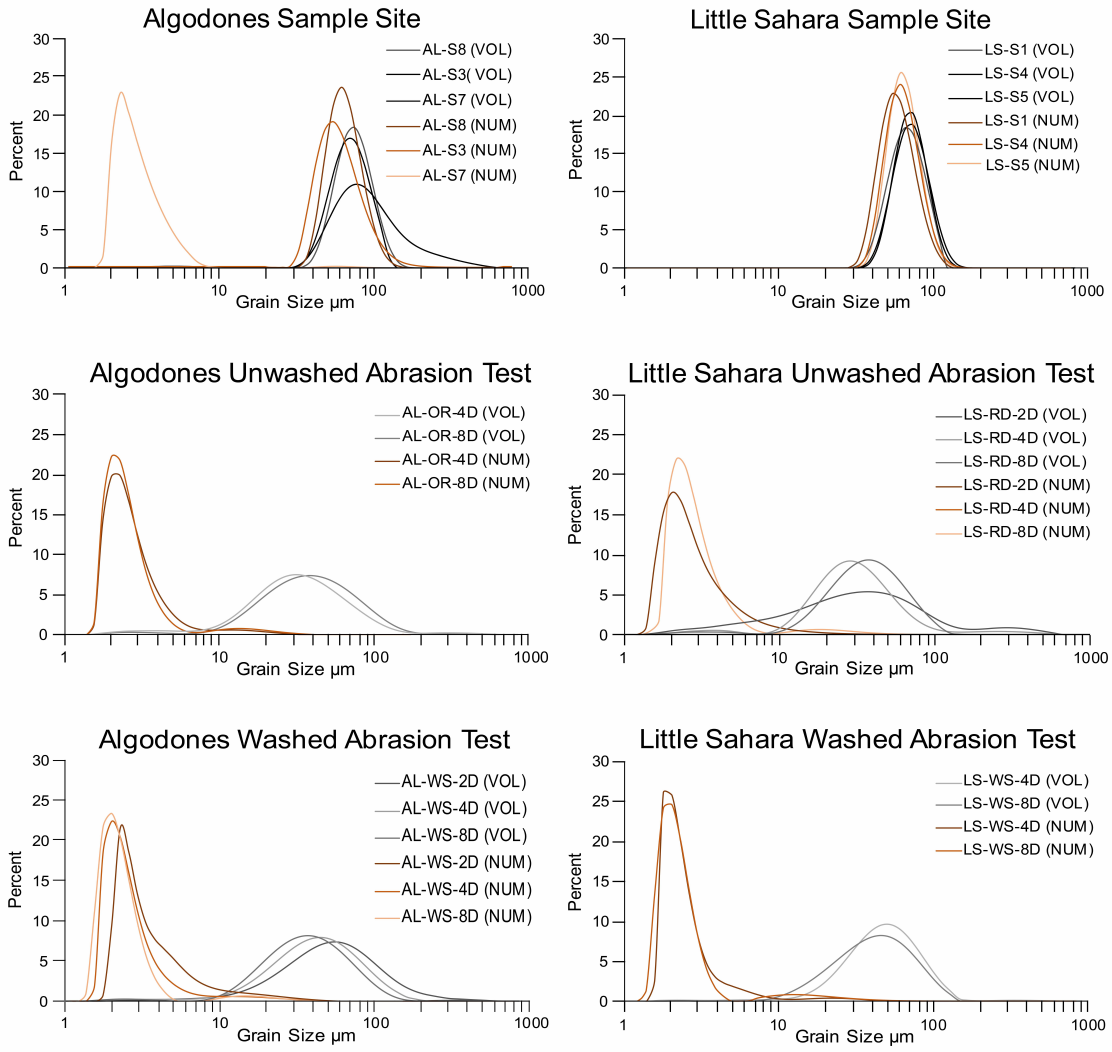

Figure 7. Silt Grain Size Distributions

Number (NUM) and volume (VOL) percent distributions of silt grains from studied samples. LS indicate Little Sahara samples. AL indicate Algodones Samples. WS indicate washed samples. OR and RD indicate unwashed samples. Field site samples are ordered in the legend from upwind to downwind. Abrasion samples are ordered in the legend by length of abrasion.

Silt Grain Size of Field Site Samples

Silt in samples collected from the Little Sahara dune field exhibits a mode range from 66 to 76 μm in volume %, indicating that grains coarser than silt or elongated grains passed through the 63 μm sieve. Mode range expressed in number % extends from 55 to 63 μm. No trend with downwind transport was observed.

Silt from the Algodones dune field exhibit a mode range (volume %) of 66 to 76 μm. Similar to the Little Sahara samples, a mode >63 μm likely reflects the passage of elongated grains through the 63 μm sieve. The number percent mode range for the Algodones field collected silt is 2.3 to 62 μm, a much wider range than that of the Little Sahara field collected silt samples. The sample site with the finest number percent mode is sample site 7 (AL-S7), which is the downwind sample.

Grain Size of Abraded Samples

Samples with masses sufficient to assess for granulometry in the LPSA are described below. Control samples, 1-day abrasion samples, and several two-day samples produced insufficient material for LPSA measurement. Unwashed Little Sahara silt samples exhibit a mode range (volume %) of 27 to 45 μm and mode range (number %) of 2.0 to 2.3 μm. Washed Little Sahara silt samples exhibit a mode range (volume %) of 45 to 52 μm and mode range (number %) from 1.7 to .2.0 μm. No trends occur between length of abrasion interval and silt grain size. Algodones unwashed silt samples exhibit a mode range (volume %) 31 to 40 μm and mode range (number %) from 2 to 2.3 μm. Washed Algodones silt samples exhibit a mode range (volume %) 58 to 35 μm and modes range (number %) from 2.0 to 2.3 μm. Volume percent mode for washed Algodones samples diminished with longer abrasion times. Number percent

mode for all abraded samples were much finer than the volume percent modes indicating a very high number of fine silt compared to a relatively low number of medium to coarse silt grains. Those larger silt grains however account for most of the volume of the samples. The volume percent mode for all abraded samples was generally similar and the number percent mode was confined to a narrow range.

Spectral Results

Results from measurements with the spectrometer show slight variation among samples both in the field and post abrasion. However, these differences have been attributed to measurement error caused by the light source of the spectrometer progressively brightening after each measurement series. When observing samples as pre-abrasion and post-abrasion pairs instead of in series the variation shrinks. Control samples and pre-abrasion starting samples showed the same trend in curve shift as post-abraded samples leading to the conclusion that the variation records a measurement error. The samples could be measured again in the future with an updated method to investigate changes in spectral profiles. The updated method would require careful spectrometer re-calibration between each sample measurement.

Remote Sensing Results

Significant changes in spectral index values were not observed for the studied indices. The Redness Index showed subtle reddening from upwind to down wind. The Iron Oxide Ratio slightly decreased from upwind to down wind. The Ferrous Minerals Ratio decreased slightly.

Figure 8. Remote Sensing Polygon Map

Map of the Algodones dune field showing the locations of polygons used to calculate the pixel count distributions for index values (RI, IOR, FMR). Four polygons along a downwind path. Polygon 1 is upwind, polygon 4 is downwind.

Redness Index

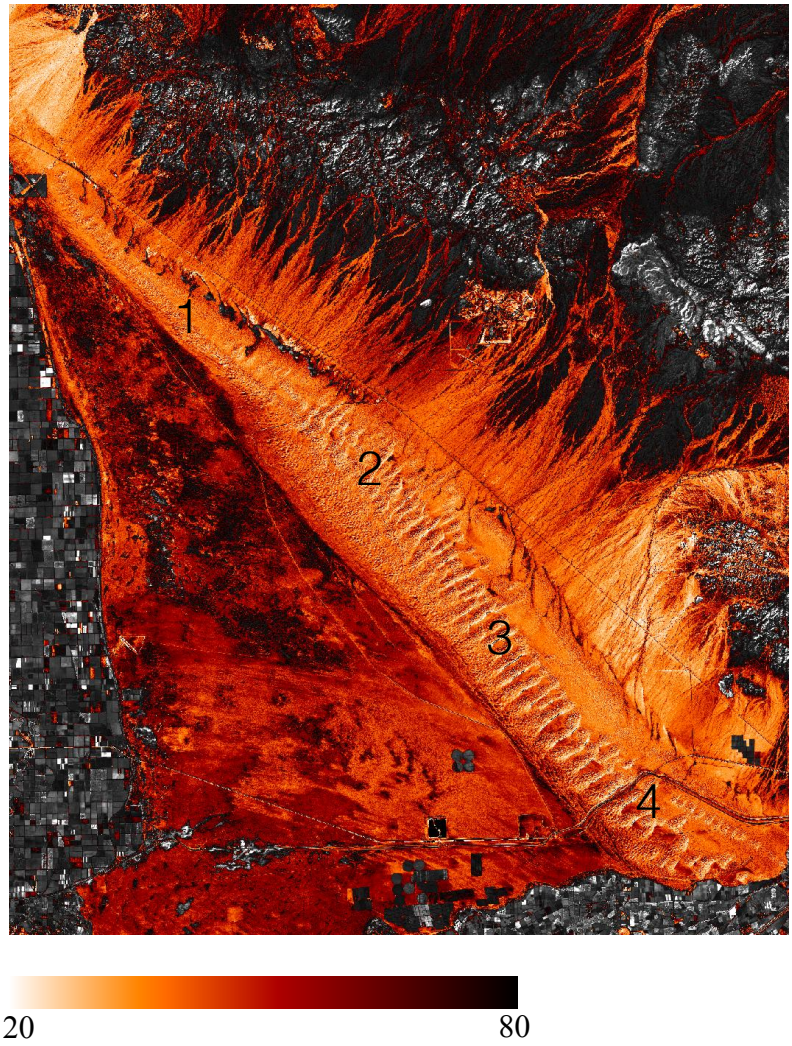

Figure 9. Redness Index Map.
Redness Index shown as a color gradient map ranging from 20 to 80. 20 is less red 80 is more red. Subtle reddening of dunes can be seen from upwind polygon (1) to downwind polygon (4).

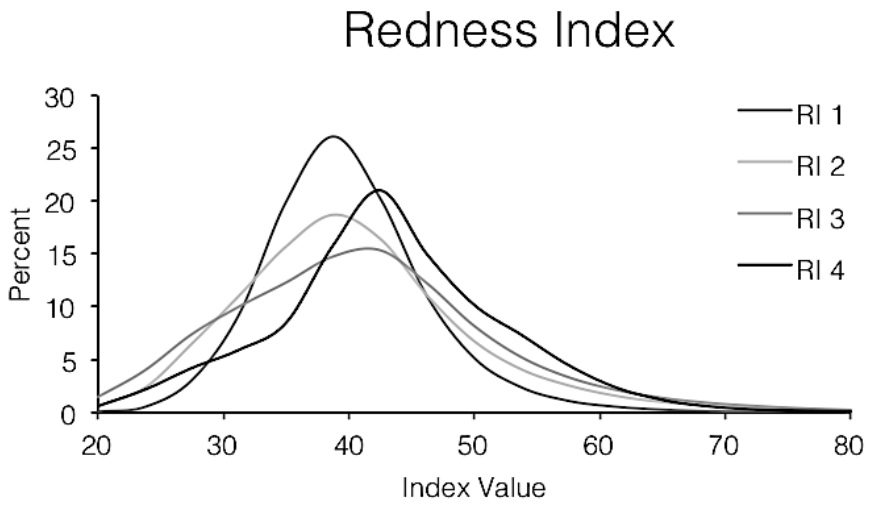

Figure 10. Redness Index Pixel Count Distributions

Pixel count distributions as a percent of total for each polygon for 16 bins. Modes for distributions have a reddening curve shift.

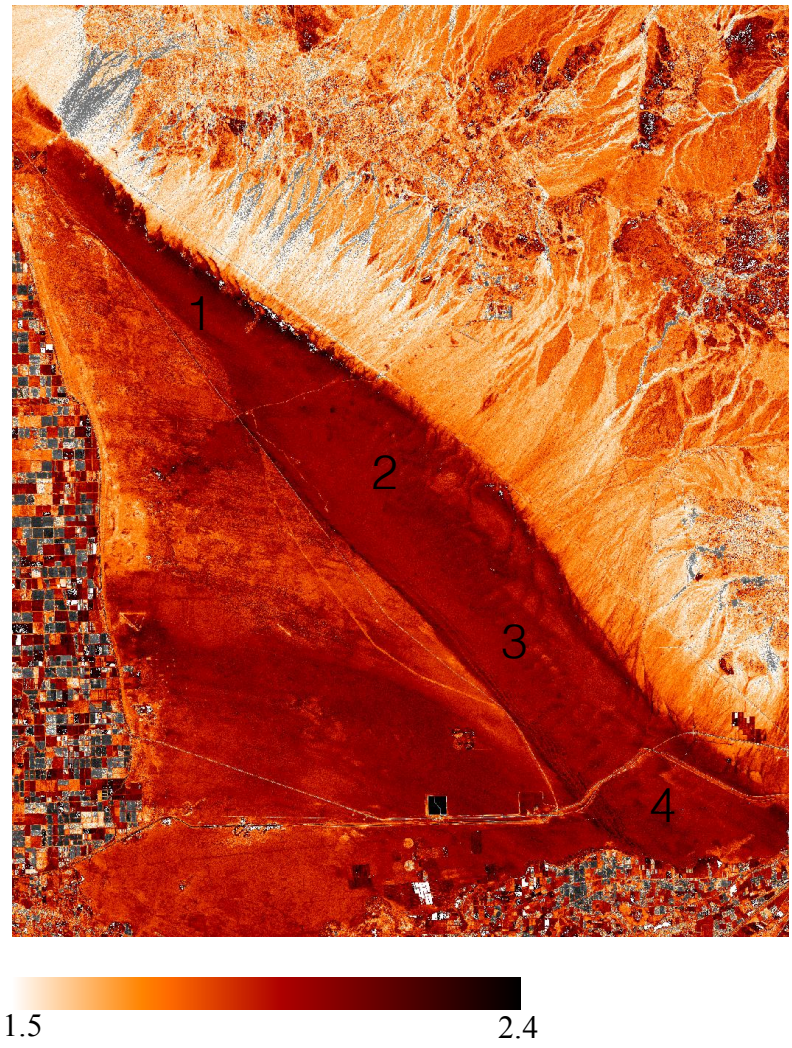

Figure 11. Iron Oxide Ratio Map

Iron Oxide Ratio values shown as a color gradient map ranging from 1.5 to 2.4. 1.5 indicating less iron oxide and 2.4 indicating higher iron oxide. No significant change is observed from the upwind polygon (1) to the down wind polygon (4)

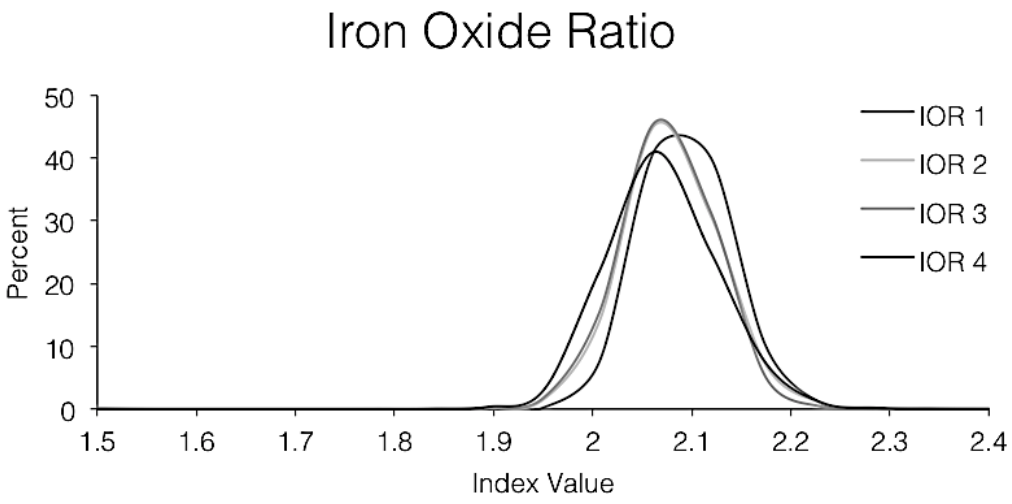

Figure 12 Iron Oxide Ratio Pixel Count Distribution

Iron Oxide Ratio pixel count distributions as a percent of the total for each polygon. Modes for distributions have a reddening shift.

Ferrous Minerals Ratio

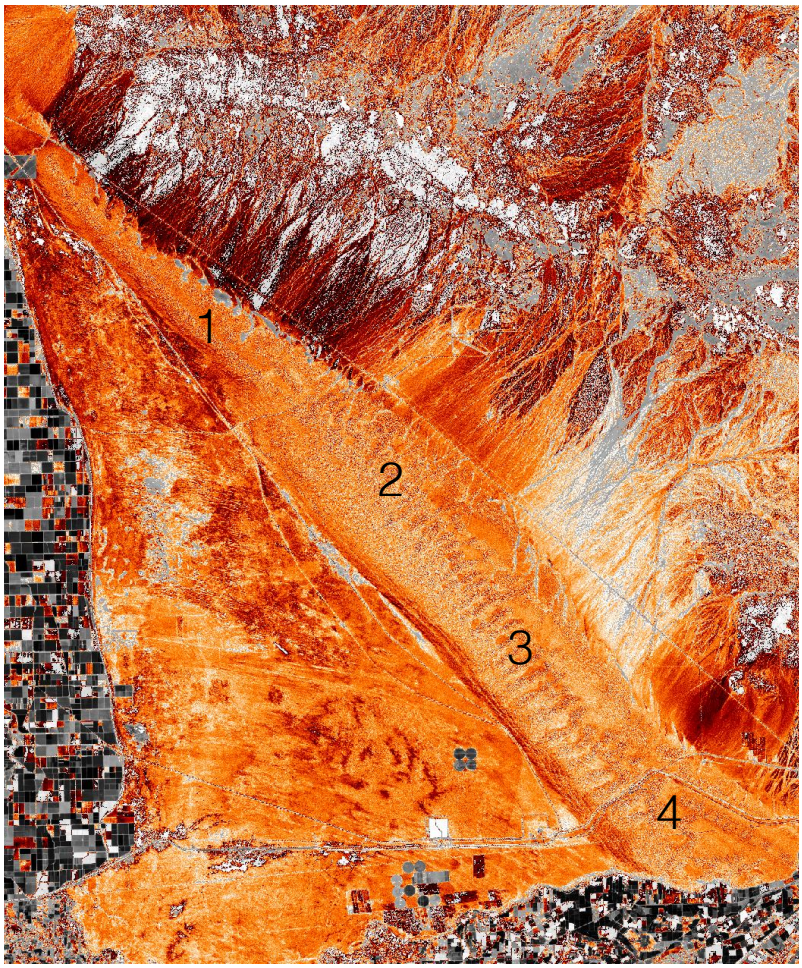

Figure 13. Ferrous Mineral Ratio Map

Ferrous Mineral Ratio values shown as a color gradient map ranging from 1.2 to 4.4. 1.2 indicating less ferrous minerals and 1.4 indicating more ferrous minerals. A small loss of ferrous minerals is observed from the upwind polygon (1) to the down wind polygon (4)

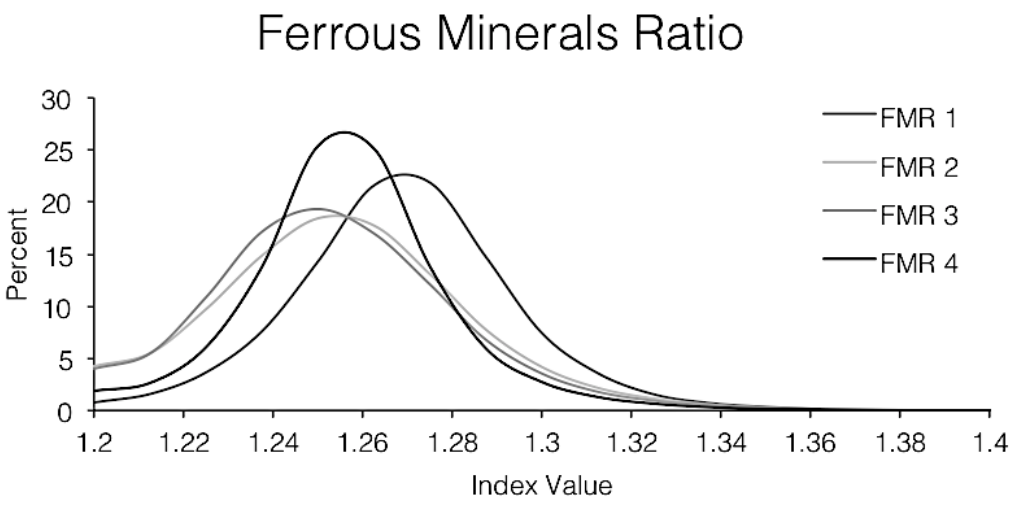

Figure 14. Ferrous Minerals Ratio Pixel Count Distribution

Ferrous Minerals Ratio pixel count distributions as a percent of the total for each polygon. Modes for distributions have a shift indicating a loss of ferrous minerals downwind.

Table 5. Scaling Results

8 days (device) = 192 years (in nature)				
Depth (cm)	Target mass % of desert	Years to target (kyr)	Accumulation rate (mm/y)	MAR (g/m2/y)
0.25	124	6400	0.0002	0.26
0.5	62.1	3200	0.0003	0.51
1	31.1	1600	0.0006	1.02
5	6.20	320	0.0031	5.12

8 days (device) = 96 years (in nature)				
Depth (cm)	Target mass % of desert	Years to target (kyr)	Accumulation rate (mm/y)	MAR (g/m2/y)
0.25	124	3200	0.0003	0.51
0.5	62.1	1600	0.0006	1.02
1	31.1	800	0.0012	2.05
5	6.20	160	0.0062	10.2

8 days (device) = 48 years (in nature)				
Depth (cm)	Target mass % of desert	Years to target (kyr)	Accumulation rate (mm/y)	MAR (g/m2/y)
0.25	124	1600	0.0006	1.02
0.5	62.1	806	0.0012	2.05
1	31.1	403	0.0025	4.09
5	6.20	80.6	0.0124	20.5

8 days (device) = 10 years (in nature)				
Depth (cm)	Target mass % of desert	Years to target (kyr)	Accumulation rate (mm/y)	MAR (g/m2/y)
0.25	124	340	0.0030	4.91
0.5	62.1	168	0.0060	9.83
1	31.1	84.0	0.0119	19.7
5	6.20	16.8	0.0595	98.3

8 days (device) = 1 year (in nature)				
Depth (cm)	Target mass % of desert	Years to target (kyr)	Accumulation rate (mm/y)	MAR (g/m2/y)
0.25	124	33.6	0.0298	49.1
0.5	62.1	16.8	0.0595	98.1
1	31.1	8.40	0.119	197
5	6.2o	1.68	0.596	983

Note: Values have been rounded and are not intended for precision estimates. The Years to target are a minimum estimate based on the input for natural time equivalence. Accumulation rates and MARs are the maximum rates estimated for the natural time equivalence.

Table 5. Scaling results ordered by length of comparative natural time to 8 days in the abrasion chamber. Depth refers to the depth of the active abrading volume in the desert. The active abrading mass is dependent on the depth of the abrading volume. The active abrading mass is proportional to the mass of the starting material in the abrasion device (100 g). Target mass % of desert refers to the mass of the target loess deposit of 1 meter. This number is displayed as a % of the active abrading mass. Years to target refers to the length of time required to accumulate the target loess deposit of 1 meter. Accumulation rate is the rate of vertical accumulation of silt in the target 1 meter loess deposit. Mass accumulation rate (MAR) is the rate of accumulation of silt by mass over one square meter per year.

Discussion

Scaling Discussion

Table 5 shows the Accumulation rates and Mass Accumulation Rates (MARs) for the different combinations of starting parameters. These values assume no loss from erosion after deposition, and assume all silt produced is deposited, which is likely an over-estimation. For the assumed abrasion volume depth of 0.25 cm the MARs calculated are lower but the same order of magnitude as regionally averaged MARs during interglacials, and significantly lower than glacial intervals reported for the Chinese Loess Plateau (CLP) (Sun et al., 2000). As the equivalent natural abrasion time is lowered, the MARs approach those reported for the CLP (Sun et al., 2000). Compared with rates linked to glacial loess deposits the scaled desert loess MARs calculated are significantly lower than those measured for the Peoria loess and the Euorpean loess, which are commonly 100 to 1000 $g/m^2/y$ and as high as 115,000 $g/m^2/y$ Frechen et al., 2003; Roberts et al., 2003). Accumulation rates for loess of the the CLP range between 0.064 mm/y and 0.145 mm/yr for the last 70 ky (Lu et al., 2007). Experimental results approach the lowest accumulation rate from Lu et al. (2007) when scaled to equate eight days of experimental abrasion to one year in nature, and using an abrading sand depth of 0.5 cm.

MARs extrapolated from the experimental results are inferred to represent a significant over-estimation even for the shallowest active abrasion depths, for the following reasons. First, the calculated MARs assume that the entire desert is being abraded with the same intensity, which is likely a substantial over-estimation because energy should vary spatially across the extent of a large desert. Second, distal rounding

and fining would likely result in a downwind reduction in abrasion potential, as angular protuberances on grains are removed. Third, modeled MARs employ the highest silt mass produced after eight days (0.0037 g), which were from washed samples, whereas natural sands are unwashed.

The calculated time required to produce a 1 m deposit at the highest rate for a 0.25 cm starting depth is 34 kyr, with a sedimentation rate of 0.03 mm/y. Lower than accumulation rates calculated for deposits on the CLP which dropped to 0.064 mm/y during interglacial stages (Lu et al., 2007). To reach the 0.5 mm/yr deposition rate needed to produce a significant loess deposit (Pye, 1984), the theoretical 1 m of silt would need to accumulate within 2000 years. Table 5 lists the conditions required for such a rate. A 5 cm abrasion depth and 192 hours of abrasion over 20 m/s annually can deposit 1 m of silt in ~1700 years. Such conditions are not considered likely to exist in nature.

Silt Mass and Grain Size

The mass of silt produced from the experimental tests was significantly lower, in terms of both total mass and percent of the starting material, compared to previous studies. Likely explanations for the difference in results include the 1) nature of the starting material, 2) mass of sand used during abrasion, and 3) abrasion energy of the experimental apparatus. This project used dune sand rather than crushed vein quartz or fluvial sands, to more realistically model a natural system, and the sand was sieved to >250 μm, to ensure exclusion of intrinsic fines. Natural dune sand used in this project was similar to sediments used by Bullard et al. (2004) in experiments that similarly produced small amounts of fines. This project used 100 g of sand as starting material,

rather than the 10 g masses used in most previous experiments (Wright et al., 1998; Bullard et al., 2004; Bullard et al., 2007). Results from Bullard et al. (2007) in a trial that used 100 g of sand produced less fine dust for the same length of abrasion time as 10 g. Bullard et al. (2007) posited that more frequent recycling of non-abraded sand in the system might explain the lower amount produced with larger starting amounts. However, if prolonged abrasion produces rounded sand grains less capable of fines production, then frequent grain cycling should provide a supply of angular sand grains with more potential for chipping and spalling. When only 10 g of sand was used in abrasion experiments the rate of fine dust production diminished with time. Larger starting samples would likely produce a constant rate for longer as appears to be the case with experiments from this project.

The energy involved in the experimental abrasion is also a controlling variable on the amount of silt produced. Lower wind speeds provide less energy for grain collisions and consequent abrasion, whereas unnaturally high wind speeds would produce more fines than expected in nature. Previous studies have not controlled for, nor measured the wind speed within the abrasion chambers. It is possible that the compressed air used in previous studies is more energetic and thus more abrasive than wind speeds experienced by dune sand under storm wind conditions. Based on testing with an anemometer the wind speed during abrasion testing does not exceed ~25 m/s for the duration of the experiment. This speed is consistent with the most energetic sustained winds experienced during average dust storms, excluding gusts (Liu et al., 2005).

Experimentally produced silt has grain size distributions consistent with previous studies that focused on the silt fraction (Wright et al., 1998; Bullard et al., 2004; Bullard et al., 2007). The volume percent mode range of experimentally produced silt (35.3 - 45.6 μm) falls within the loess range of typical Peoria loess (Wang et al., 2006). The experimentally produced silt has a coarser mode than typical CLP loess (~25 μm) and is finer than silt deposited at north African desert margins (~60 μm) (Assallay, et al., 1998) The volume-percent modes of produced silt are finer than the silt contained within the natural dune sites. Mode ranges for silt collected from dune field sample sites were coarse and in the range of desert margin silt deposits. Volume percent and number percent differ in experimental results because produced fines are confined to the abrasion chamber and cannot be transported away as they would in an open desert. The most distal sample location (AL-S7) in the Algodones dune field exhibits a number percent mode (2.3 μm) finer than the volume percent mode (66.9 μm), similar to experimental results. The fines causing the shifted number percent were likely transported from upwind and are potentially products of abrasion in the desert. Distal Algodones dunes did not have a grain size mode in the 35 – 50 μm range which would be expected if the down wind dunes were accumulating the medium to coarse silt produced in the desert. The lack of a grain size mode similar in scale to the abrasion produced silt could be from a lack of abrading wind energy in the Algodones dune field.

Conclusion

A new experimental device was used to abrade natural dune sands for durations of up to 8 days in simulated constant storm-wind conditions. The produced fines were of insufficient mass to measure reflectance values with a spectrometer, thus precluding comparison of spectral properties of autochthonous versus allochthonous desert silt. Spectral reflectance data of sand from sample sites and experimental abrasion proved unreliable for assessing fate of grain coatings during desert abrasion. Removal of clay coatings was observed during abrasion experiments.

Remote sensing investigations revealed no substantial variation in dune spectral properties with down-wind distance, suggesting that alteration of dune color spatially and temporally is likely climate dependent. Slight reddening of dunes downwind matches observations by Walker (1979) regarding reddening of dunes with transport distance in the extremely arid climate of Libya. It is possible that formation of grain coatings at the Algodones dune site is counterbalanced by loss of coatings from mechanical abrasion, thus producing little spectral change with transport distance.

Relative to previous studies, experimental abrasion produced only minimal fines. Production rates were scaled to maximize potential depositional rates in nature and to investigate which variables influenced accumulation. Scaling up the rate of fines production to spatial and temporal dimensions typical in nature suggests that sand saltation in deserts is unlikely to produce geologically significant loess deposits. Experimental aeolian abrasion produced silt in the loess grain size range of 20 to 60 μm with modes ranging from 35.3 - 45.6 μm. Results indicate that, although silt in loess

deposits could contain a fraction of material produced from aeolian saltation of sand, the majority of silt in loess deposits likely originated via other processes.

References

Assallay, A.M., Rogers, C.D.F., Smalley, I.J., and Jefferson, I.F., 1998, Silt: 2 - 62μm 9 - 4ø Earth Science Reviews, v. 45, p. 61–88, doi: 10.1016/S0012-8252 (98) 00035 - X.

Ben-Dor, E., Levin, N., Singer, A., Karnieli, A., Braun, O., and Kidron, G.J., 2006, Quantitative mapping of the soil rubification process on sand dunes using an airborne hyperspectral sensor: Geoderma, v. 131, p. 1–21, doi: 10.1016/j.geoderma.2005.02.011.

Bettis, E.A., Muhs, D.R., Roberts, H.M., and Wintle, A.G., 2003, Last Glacial loess in the conterminous USA: Quaternary Science Reviews, v. 22, p. 1907–1946, doi: 10.1016/S0277-3791(03)00169-0.

Bullard, J.E., Mctainsh, G.H., and Pudmenzky, C., 2007, Factors affecting the nature and rate of dust production from natural dune sands: Sedimentology, v. 54, p. 169–182, doi: 10.1111/j.1365-3091.2006.00827.x.

Bullard, J.E., McTainsh, G.H., and Pudmenzky, C., 2004, Aeolian abrasion and modes of fine particle production from natural red dune sands: An experimental study: Sedimentology, v. 51, p. 1103–1125, doi: 10.1111/j.1365-3091.2004.00662.x.

Bullard, J.E., and White, K., 2005, Dust production and the release of iron oxides resulting from the aeolian abrasion of natural dune sands: Earth Surface Processes and Landforms, v. 30, p. 95–106, doi: 10.1002/esp.1148.

Cheng, J. jun, Jiang, F. qiang, Xue, C. xiao, Xin, G. wei, Li, K. chong, and Yang, Y. hai, 2015, Characteristics of the disastrous wind-sand environment along railways in the Gobi area of Xinjiang, China: Atmospheric Environment, v. 102, p. 344–354, doi: 10.1016/j.atmosenv.2014.12.018.

Crouvi, O., Amit, R., Enzel, Y., and Gillespie, A.R., 2010, Active sand seas and the formation of desert loess: Quaternary Science Reviews, v. 29, p. 2087–2098, doi: 10.1016/j.quascirev.2010.04.026.

Derickson, D., Kocurek, G., Ewing, R.C., and Bristow, C., 2008, Origin of a complex and spatially diverse dune-field pattern, Algodones, southeastern California: Geomorphology, v. 99, p. 186–204, doi: 10.1016/j.geomorph.2007.10.016.

ESA, 2015, Sentinel-2 User Handbook, v. 1.2 p. 1-64.

Frechen, M., Oches, E.A., and Kohfeld, K.E., 2003, Loess in Europe—mass accumulation rates during the Last Glacial Period: Quaternary Science Reviews, v. 22, p. 1835–1857, doi: 10.1016/S0277-3791(03)00183-5.

Ghrefat, H.A., Goodell, P.C., Hubbard, B.E., Langford, R.P., and Aldouri, R.E., 2007, Modeling grain size variations of aeolian gypsum deposits at White Sands, New Mexico, using AVIRIS imagery: Geomorphology, v. 88, p. 57–68, doi: 10.1016/j.geomorph.2006.10.013.

Goudie, A.S., and Middleton, N.J., 2001, Saharan dust storms: Nature and consequences: Earth-Science Reviews, v. 56, p. 179–204, doi: 10.1016/S0012-8252(01)00067-8.

Kuenen, P.H., 1960, Experimental Abrasion 4 : Eolian Action: The Journal of Geology, v. 68, p. 427–449.

Kok, J.F., and Renno, N.O., 2008, Electrostatics in wind-blown sand: Physical Review Letters, v. 100, doi: 10.1103/PhysRevLett.100.014501.

Kok, J., Parteli, E., Michaels, T., and Karam, D., 2012, The physics of wind blown sand and dust: Reports on Progress in Physics, v. 75, p. 106901, http://iopscience.iop.org/article/10.1088/0034-4885/75/10/106901/pdf (accessed April 2018).

Lepper, K., and Scott, G.F., 2005, Late Holocene aeolian activity in the Cimarron River valley of west-central Oklahoma: Geomorphology, v. 70, p. 42–52, doi: 10.1016/j.geomorph.2005.03.010.

Leu, D.J., 1977, Visible and Near - Infrared Reflectance of Beach Sands : A Study on the Spectral Reflectance Grain Size Relationship: v. 182, p. 169–182.

Li, J., Okin, G.S., Herrick, J.E., Belnap, J., Munson, S.M., and Miller, M.E., 2010, A simple method to estimate threshold friction velocity of wind erosion in the field: Geophysical Research Letters, v. 37, p. n/a-n/a, doi: 10.1029/2010GL043245.

Liu, L.Y., Skidmore, E., Hasi, E., Wagner, L., and Tatarko, J., 2005, Dune sand transport as influenced by wind directions, speed and frequencies in the Ordos Plateau, China: Geomorphology, v. 67, p. 283–297, doi: 10.1016/J.GEOMORPH.2004.10.005.

Lu, Y.C., Wang, X.L., and Wintle, A.G., 2007, A new OSL chronology for dust accumulation in the last 130,000 yr for the Chinese Loess Plateau: Quaternary Research, v. 67, p. 152–160, doi: 10.1016/J.YQRES.2006.08.003.

Lumini ONE Spectrometric Camera, Myspectral, myspectral.com/product/lumini-one/. 2008.

Lv, Y., and Sun, Z., 2016, Multi-angular spectral reflectance to characterize the particle size of surfaces of desert and cultivated soil: European Journal of Soil Science, v. 67, p. 253–265, doi: 10.1111/ejss.12341.

Mathieu, R., Pouget, M., Cervelle, B., and Escadafal, R., 1998, Relationships between satellite-based radiometric indices simulated using laboratory reflectance data and typic soil color of an arid environment: Remote Sensing of Environment, v. 66, p. 17–28, doi: 10.1016/S0034-4257(98)00030-3.

Muhs, D.R., Bush, C.A., Cowherd, S.D., and Mahan, S., 1995, Geomorphic and geochemical evidence for the source of sand in the Alogdones Dunes, Colorado Desert, southeastern California: Desert Aeolian Processes, p. 37–74, doi: 10.1007/978-94-009-0067-7_3.

Muhs, D.R., 2013, The geologic records of dust in the quaternary: Aeolian Research, v. 9, p. 3–48, doi: 10.1016/j.aeolia.2012.08.001.

Norris, R.M., And Norris, K.S., 1961, Algodones Dunes of Southeastern California: Geological Society of America Bulletin, v. 72, p. 605 LP-619, http://gsabulletin.gsapubs.org/content/72/4/605.abstract.

Okin, G.S., and Painter, T.H., 2004, Effect of grain size on remotely sensed spectral reflectance of sandy desert surfaces: Remote Sensing of Environment, v. 89, p. 272–280, doi: 10.1016/j.rse.2003.10.008.

Pullen, A., Kapp, P., McCallister, A.T., Chang, H., Gehrels, G.E., Garzione, C.N., Heermance, R. V., and Ding, L., 2011, Qaidam Basin and northern Tibetan Plateau as dust sources for the Chinese Loess Plateau and paleoclimatic implications: Geology, v. 39, p. 1031–1034, doi: 10.1130/G32296.1.

Pye, K., 1984, Loess: Progress in Physical Geography, v. 8, p. 176–217.

Pye, K., 1995, The nature, origin and accumulation of loess: Quaternary Science Reviews, v. 14, p. 653–667, doi: 10.1016/0277-3791(95)00047-X.

Pye, K., and Tsoar, H., 2013, Aeolian sand and sand dunes: v. 53, doi: 10.1017/CBO9781107415324.004.

Roberts, H.M., Muhs, D.R., Wintle, A.G., Duller, G.A.T., and Bettis, E.A., 2003, Unprecedented last-glacial mass accumulation rates determined by luminescence dating of loess from western Nebraska: Quaternary Research, v. 59, p. 411–419, doi: 10.1016/S0033-5894(03)00040-1.

Rogers, B., 2000, Morphology Of Fixed Sand Dunes For Paleowind Reconstruction In Northwestern Oklahoma By: Oklahoma State University.

Roskin, J., Blumberg, D.G., Porat, N., Tsoar, H., and Rozenstein, O., 2012, Do dune sands redden with age? The case of the northwestern Negev dunefield, Israel: Aeolian Research, v. 5, p. 63–75, doi: 10.1016/j.aeolia.2011.11.004.

Smalley, I.J., and Vita-Finzi, C., 1968, The Formation Of Fine Particles In Sandy Deserts And The Nature Of 'Desert ~ Loess 1: Journal Of Sedimentary Petrology, v. 38, p. 76–1.

Smalley, I., 1995, Making the material: The formation of silt sized primary mineral particles for loess deposits: Quaternary Science Reviews, v. 14, p. 645–651, doi: 10.1016/0277-3791(95)00046-1.

Smalley, I.J., Kumar, R., O'Hara Dhand, K., Jefferson, I.F., and Evans, R.D., 2005, The formation of silt material for terrestrial sediments: Particularly loess and dust: Sedimentary Geology, v. 179, p. 321–328, doi: 10.1016/j.sedgeo.2005.06.011.

Smith, B.J., Wright, J.S., and Whalley, W.B., 2002, Sources of non-glacial, loess-size quartz silt and the origins of "desert loess": Earth-Science Reviews, v. 59, p. 1–26, doi: 10.1016/S0012-8252(02)00066-1.

Smith, B.J., Wright, J.S., and Whalley, W.B., 1991, Simulated aeolian abrasion of Pannonian sands and its implications for the origins of Hungarian loess: Earth Surface Processes and Landforms, v. 16, p. 745–752, doi: 10.1002/esp.3290160808.

SNAP - ESA Sentinel Application Platform v6.0, http://step.esa.int

Stokes, S., Kocurek, G., Pye, K., and Winspear, N.R., 1997, New evidence for the timing of aeolian sand supply to the Algodones dunefield and East Mesa area, southeastern California, USA: Palaeogeography, Palaeoclimatology, Palaeoecology, v. 128, p. 63–75, doi: 10.1016/S0031-0182(96)00048-X.

Sun, J.M., Kohfeld, K.E., and Harrison, S.P., 2000, Records of aeolian dust deposition on the Chinese Loess Plateau during the Late Quaternary: Max-Planck-Institute fur Biogeochemie, 327 p., doi: 10.4126/98-004424382.

Tsoar, H., And Pye, K., 1987, Dust transport and the question of desert loess formation: Sedimentology, v. 34, p. 139–153, doi: 10.1111/j.1365-3091.1987.tb00566.x.

van der Meer, F.D., van der Werff, H.M.A., van Ruitenbeek, F.J.A., Hecker, C.A., Bakker, W.H., Noomen, M.F., van der Meijde, M., Carranza, E.J.M., Smeth, J.B. de, and Woldai, T., 2012, Multi- and hyperspectral geologic remote sensing: A review: International Journal of Applied Earth Observation and Geoinformation, v. 14, p. 112–128, doi: 10.1016/J.JAG.2011.08.002.

Walker, T.R., 1979, A study of global sand seas: Red color in dune sand, in McKee, E.D., ed., A study of global sand seas : U.S. Geological Survey Professional Paper P 105, p. 61–81.

Wang, H., Mason, J.A., and Balsam, W.L., 2006, The importance of both geological and pedological processes in control of grain size and sedimentation rates in

Peoria Loess: Geoderma, v. 136, p. 388–400, doi: 10.1016/j.geoderma.2006.04.005.

Whalley, W.B., Smith, B.J., McAlister, J.J., and Edwards, A.J., 1987, Aeolian abrasion of quartz particles and the production of silt-size fragments: preliminary results: Geological Society, London, Special Publications, v. 35, p. 129–138, doi: 10.1144/GSL.SP.1987.035.01.09.

White, K., and Bullard, J., 2009, Abrasion control on dune colour: Muleshoe Dunes, SW USA: Geomorphology, v. 105, p. 59–66, doi: 10.1016/j.geomorph.2008.01.019.

Wright, J., Smith, B., and Whalley, B., 1998, Mechanisms of loess-sized quartz silt production and their relative effectiveness: laboratory simulations: Geomorphology, v. 23, p. 15–34, doi: 10.1016/S0169-555X(97)00084-6.

Wright, J., 2001a, Making loess-sized quartz silt: Data from laboratory simulations and implications for sediment transport pathways and the formation of "desert" loess deposits associated with the Sahara: Quaternary International, v. 76–77, p. 7–19, doi: 10.1016/S1040-6182(00)00085-9.

Wright, J.S., 2001b, Desert loess versus glacial loess: Quartz silt formation, source areas and sediment pathways in the formation of loess deposits: Geomorphology, v. 36, p. 231–256, doi: 10.1016/S0169-555X(00)00060-X.

Wright, J.S., 2007, An overview of the role of weathering in the production of quartz silt: Sedimentary Geology, v. 202, p. 337–351, doi: 10.1016/j.sedgeo.2007.03.024.

Yang, Y.Y., Qu, Z.Q., Shi, P.J., Liu, L.Y., Zhang, G.M., Tang, Y., Hu, X., Lv, Y.L., Xiong, Y.Y., Wang, J.P., Shen, L.L., Lv, L.L., and Sun, S., 2014, Wind regime and sand transport in the corridor between the Badain Jaran and Tengger deserts, central Alxa Plateau, China: Aeolian Research, v. 12, p. 143–156, doi: 10.1016/j.aeolia.2013.12.006.

Yao, Z., Xiao, J., and Jiang, F., 2012, Characteristics of daily extreme-wind gusts along the Lanxin Railway in Xinjiang, China: Aeolian Research, v. 6, p. 31–40, doi: 10.1016/j.aeolia.2012.07.002.

Zijiang, Z., and Xiwen, W., 2002, Analysis of the severe group dust storms in eastern part of Northwest China: Journal of Geographical Sciences, v. 12, p. 357–362, https://link.springer.com/content/pdf/10.1007/BF02837557.pdf (accessed April 2018).

Appendix A: Silt Photos and Additional Grain Size Distribution Figures

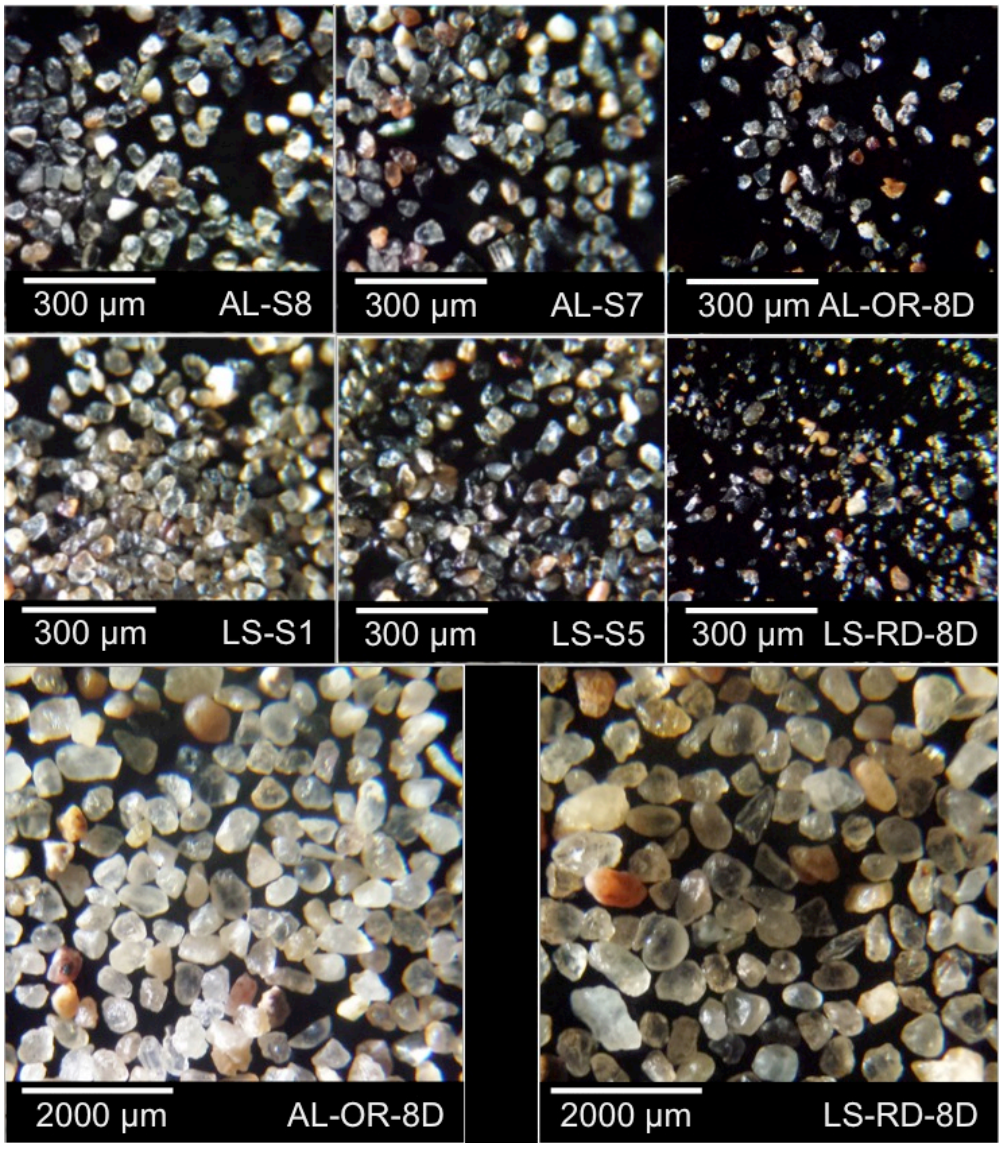

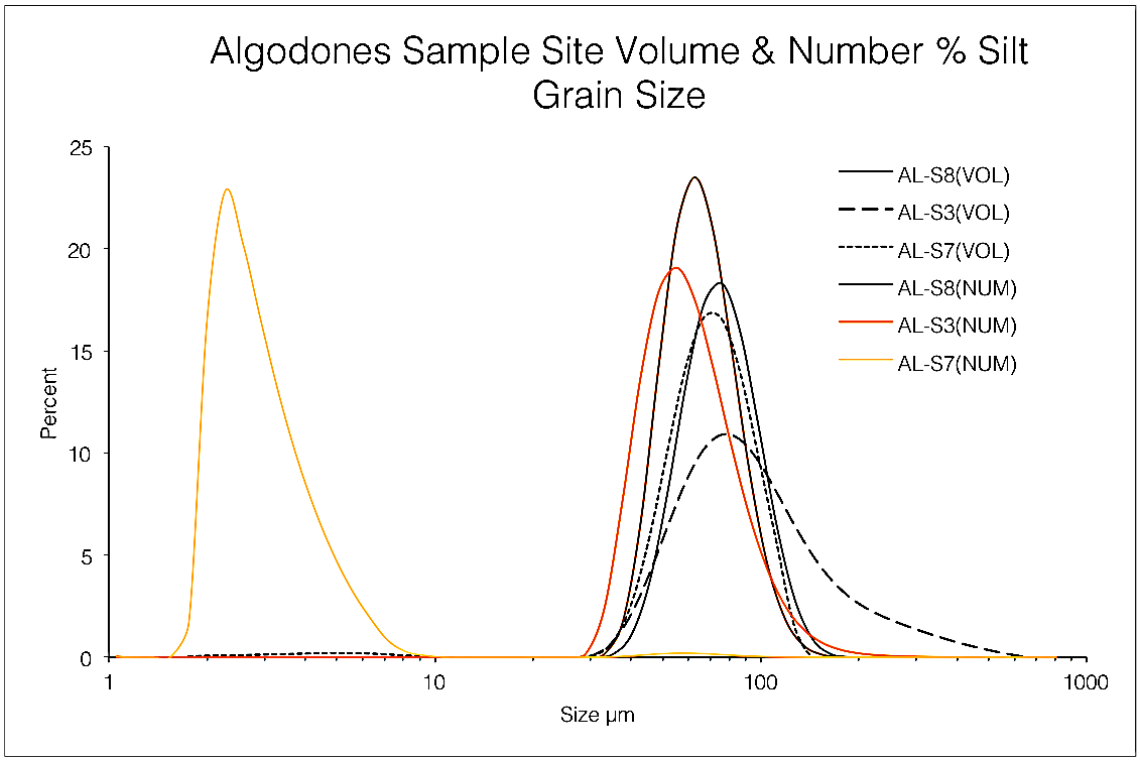
Algodones Sample Site Volume & Number % Silt Grain Size
Percent
25
20
15
10
5
0
1
10
100
1000
Size µm
AL-S8(VOL)
AL-S3(VOL)
AL-S7(VOL)
AL-S8(NUM)
AL-S3(NUM)
AL-S7(NUM)

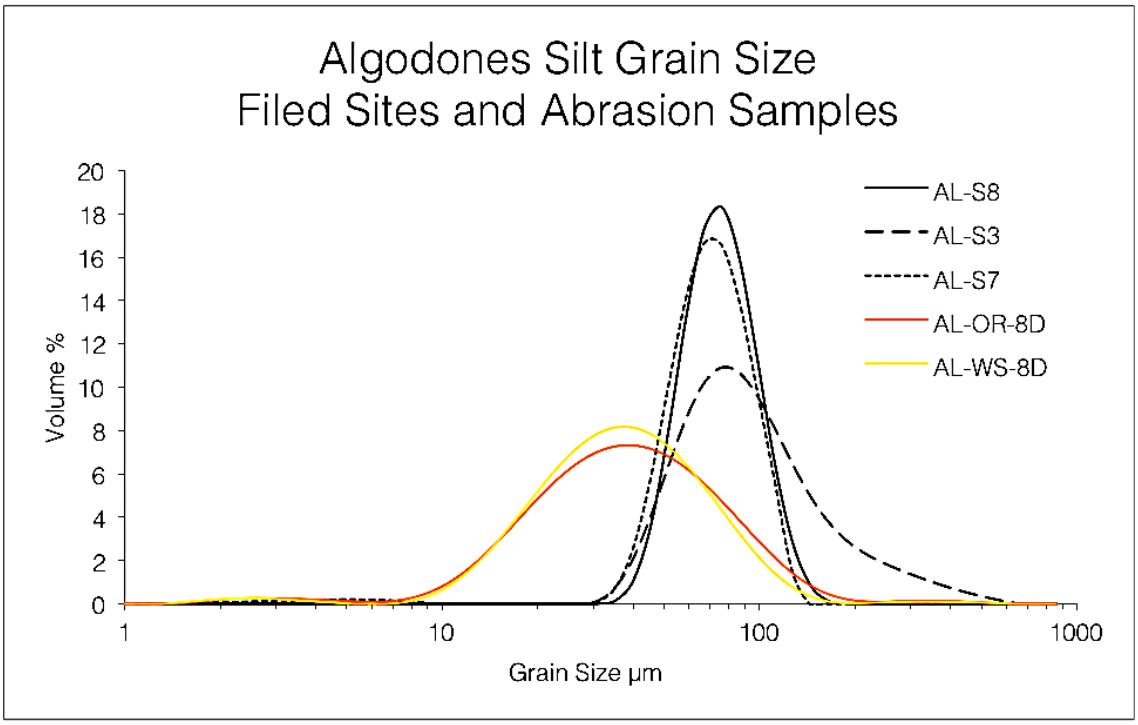
Algodones Silt Grain Size
Filed Sites and Abrasion Samples
Volume %
20
18
16
14
12
10
8
6
4
2
0
1
10
100
1000
Grain Size µm
AL-S8
AL-S3
AL-S7
AL-OR-8D
AL-WS-8D

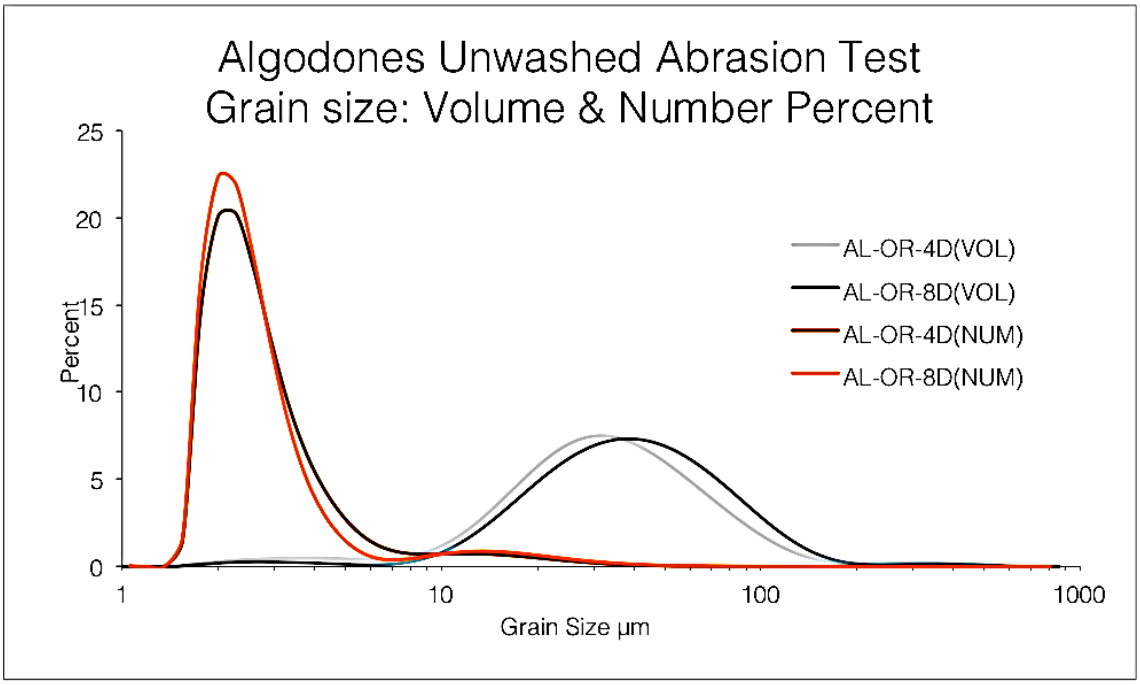
Algodones Unwashed Abrasion Test
Grain size: Volume & Number Percent
Percent
25
20
15
10
5
0
1
10
100
1000
Grain Size µm
AL-OR-4D(VOL)
AL-OR-8D(VOL)
AL-OR-4D(NUM)
AL-OR-8D(NUM)

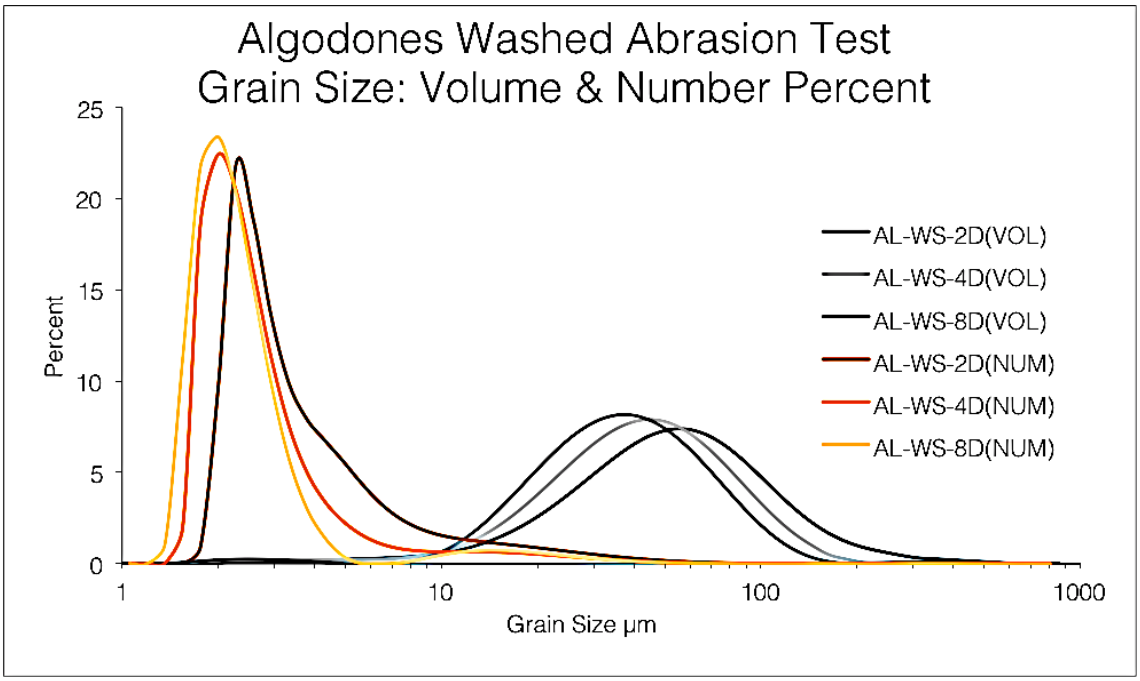
Algodones Washed Abrasion Test
Grain Size: Volume & Number Percent
Percent
25
20
15
10
5
0
1
10
100
1000
Grain Size µm
AL-WS-2D(VOL)
AL-WS-4D(VOL)
AL-WS-8D(VOL)
AL-WS-2D(NUM)
AL-WS-4D(NUM)
AL-WS-8D(NUM)

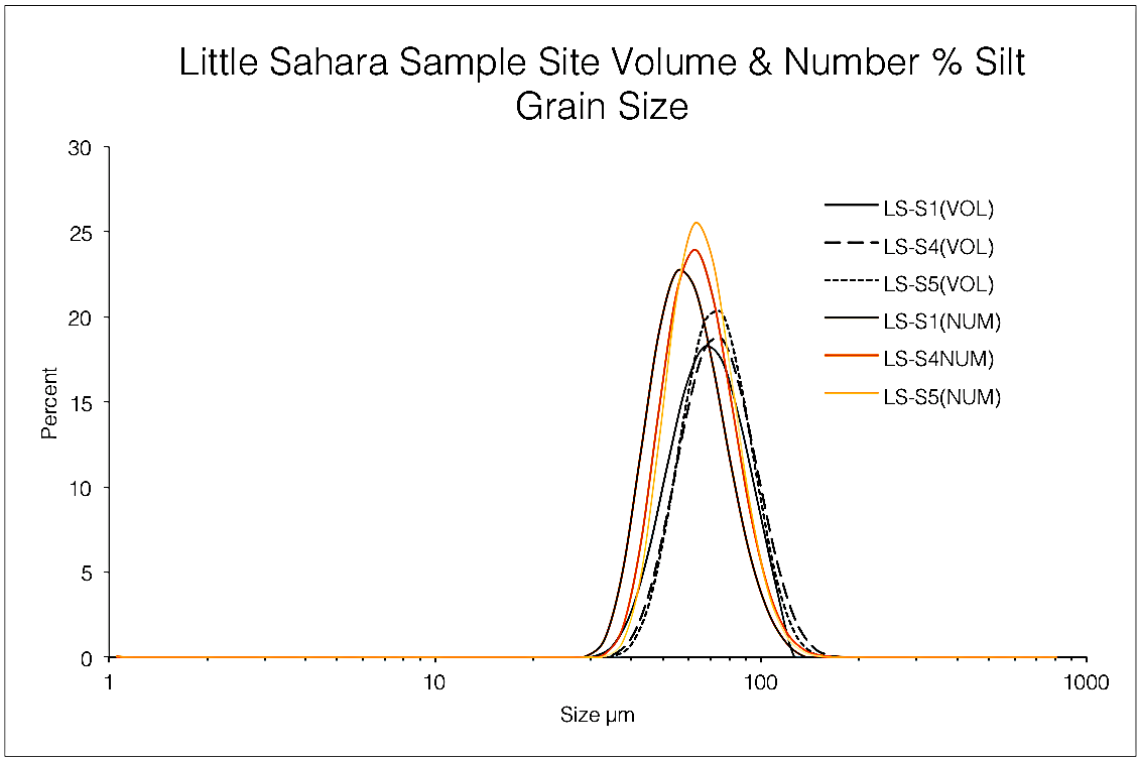
Little Sahara Sample Site Volume & Number % Silt Grain Size
Percent
30
25
20
15
10
5
0
1
10
100
1000
Size µm
LS-S1(VOL)
LS-S4(VOL)
LS-S5(VOL)
LS-S1(NUM)
LS-S4NUM)
LS-S5(NUM)

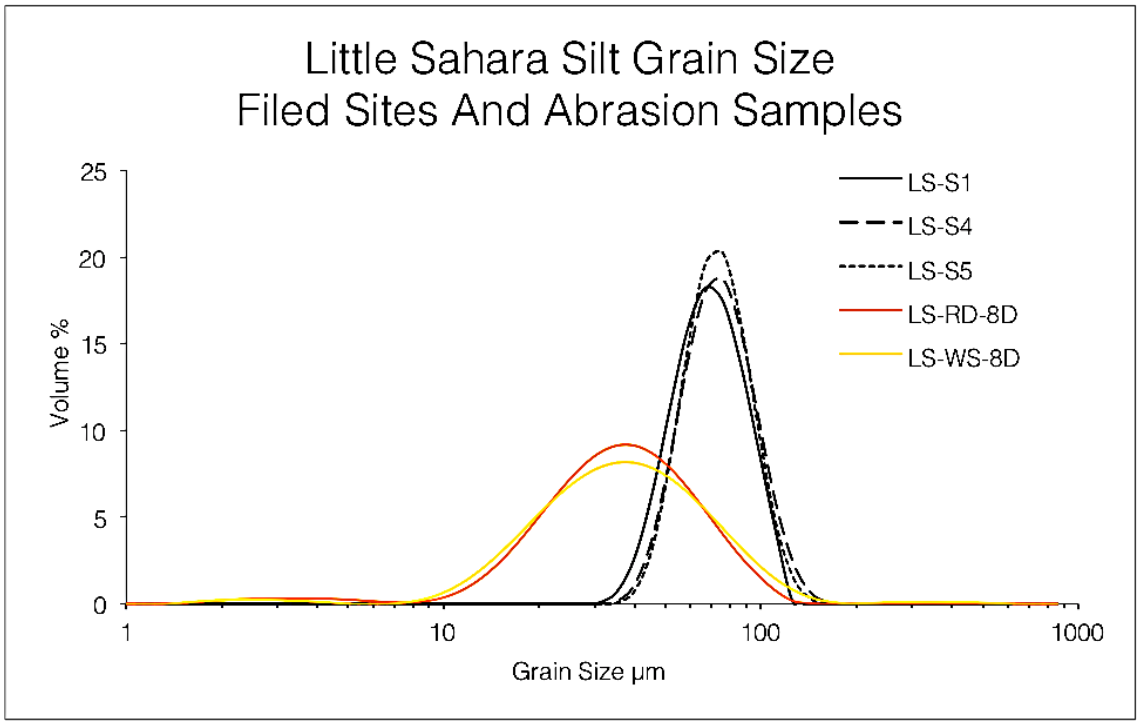
Little Sahara Silt Grain Size
Filed Sites And Abrasion Samples
25
20
15
10
5
0
Volume %
1
10
100
1000
Grain Size µm
LS-S1
LS-S4
LS-S5
LS-RD-8D
LS-WS-8D

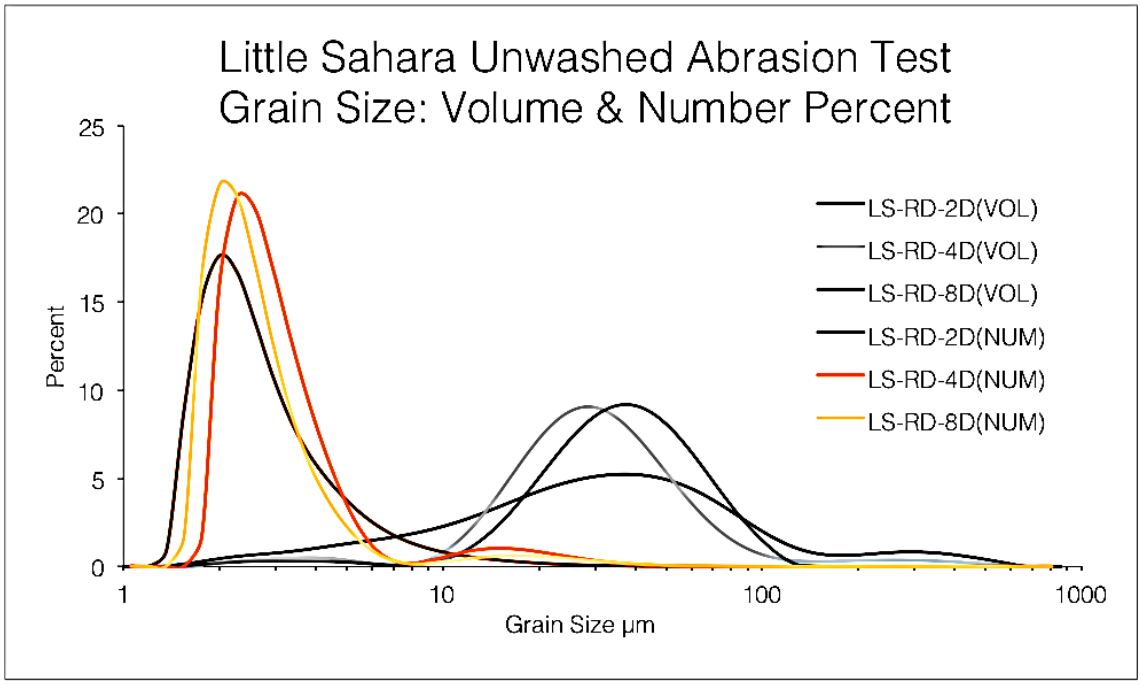
Little Sahara Unwashed Abrasion Test
Grain Size: Volume & Number Percent
Percent
25
20
15
10
5
0
1
10
100
1000
Grain Size µm
LS-RD-2D(VOL)
LS-RD-4D(VOL)
LS-RD-8D(VOL)
LS-RD-2D(NUM)
LS-RD-4D(NUM)
LS-RD-8D(NUM)

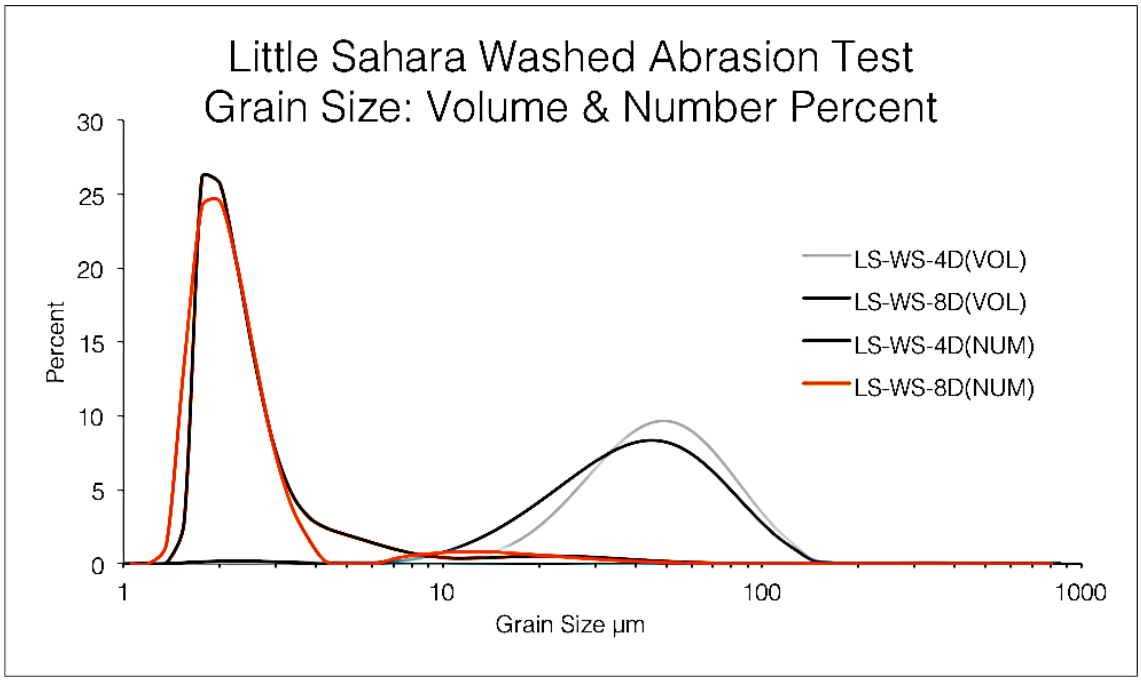
Little Sahara Washed Abrasion Test
Grain Size: Volume & Number Percent
Percent
30
25
20
15
10
5
0
1
10
100
1000
Grain Size µm
LS-WS-4D(VOL)
LS-WS-8D(VOL)
LS-WS-4D(NUM)
LS-WS-8D(NUM)